


CAIF & ASI Final Report

Spacecraft Dynamics Employing a General Multi-tank and Multi-thruster Mass Depletion Formulation

---

Author:
Mr. Paolo Panicucci

Supervisor:
Dr. Hanspeter Schaub

Version 1.0 of
October 11, 2016

Acknowledgments

The present research work has been founded by a grant for the summer 2016 offered by the ASI (Italian Space Agency) with the participation of the CAIF (Cultural Association of Italians at Fermilab) that gave me the opportunity to enjoy and experience a fruitful period in the AVSLab (Autonomous Vehicle System Laboratory) at the Colorado University in Boulder.
I would like to thank my supervisor Hanspeter Schaub both for the possibility he gave me to work in his laboratory and to join his research group at the AVSLab and for his availability in sharing his knowledge about interesting and various topics to solve all my doubts.
A special thanks goes to Prof. Simone Donati and Prof. Giorgio Bellettini for the help in managing the grant and in supporting me with helpful technical advice about the visa and the flight.
I sincerely and strongly support any future realization of the present program as it is a real and practical opportunity both to incentive the international mobility among universities and to join the Italian expertise and the American experience in the research sector to create future and interesting collaborations.

Abstract

Having high fidelity numerical simulations for the dynamics of a spacecraft is becoming increasingly important for space missions. Constraints are becoming more and more stringent as far as precision attitude pointing, attitude jitter, and orbital accuracy are concerned. A crucial aspect of spacecraft dynamics is the depleting mass due to thrusters. Orbital maneuvers and Dynamics and Control (ADC) nozzles firing change the current spacecraft mass properties and results in an associated reaction force and torque. To perform orbital and attitude control using thrusters, or to obtain optimal trajectories, the impact of mass variation and depletion of the spacecraft must be thoroughly understood. Earlier works make many assumptions while deriving the equations of motion, such as considering an axial symmetric body or a given tank's geometry, that could decrease the generality and applicability of the models and result in the necessity to re-derive equations of motion for specific spacecraft.

This paper develops the fully coupled translational and rotational equations of motion of a spacecraft that is ejecting mass through the use of thrusters. The derivation begins considering the entire closed system: the spacecraft and the ejected fuel. Then the exhausted fuel motion in free space is expressed using the thruster nozzle properties and the well-known thrust vector to avoid tracking the expelled fuel in the simulation. The present formulation considers a general multi-tank and multi-thruster approach to account for both the depleting fuel mass in the tanks and the one exiting the thruster nozzles. General spacecraft configurations are possible where thrusters can pull a single, multiple tanks, or the tank being drawn from can be switched via a valve.

To perform validation of the model developed and to show the impact of

assumptions that are made for mass depletion in other models, numerical simulations are presented and compared to a simple parameters-update approach. Additionally, an orbital maneuver with attitude control is included and the impact on mass variation is taken into account by updating the mass flow of each ADC nozzle.

Contents

List of Figures

List of Tables

1 Introduction

In the space sector the increase in accuracy and high-fidelity simulations are strongly pushing the limits to achieve simulation test bench for spacecraft systems. The prediction of satellite behaviors and their orbits during the preliminary phase design or, at least before the integration and operational period, can be a way to limit the errors in pointing and attitude jitter. Moreover, high-fidelity models could provide a efficient way to limit fuel demanding maneuvers to preserve satellite orbital position.
This report will present firstly how the equations of motion (EOMs) have been mathematically inferred from dynamical principals, such as the Newton's second law. Secondly, a control strategy will be exposed in order to limit the attitude error in pointing and angular velocity of the satellite about its control reference frame. Thirdly, the developed nozzles and tanks model will be explained and their mathematical relations established. Finally. results and conclusion will be presented to underline importance of considering the previously exposed phenomena to obtain close-to-reality simulations and high-accuracy model.

2 Notations and reference frames

The following notations will be used:

- $\boldsymbol{r}_{C/N}$ is the vector pointing from N to C.
- ${}^{\mathcal{B}}\boldsymbol{r}$ is the vector $\boldsymbol{r}$ expressed in the $\mathcal{B}$ reference frame.
- $\boldsymbol{\omega}_{\mathcal{B}/\mathcal{N}}$ is the angular velocity of the $\mathcal{B}$ reference frame about the $\mathcal{N}$ one.
- $\boldsymbol{r}'$ denotes the derivate with respect to the time in the body fixed reference frame.
- $\dot{\boldsymbol{r}}$ denotes the derivate with respect to the time in the $\mathcal{N}$ reference frame.

Moreover, different reference frames will be presented to model properly the problem:

- The inertial reference frame $\mathcal{N}$ centered in N and oriented freely in space.
- The body fixed reference frame $\mathcal{B}$ with origin B and versors $\{\hat{\boldsymbol{b}}_1\,,\hat{\boldsymbol{b}}_2\,,\hat{\boldsymbol{b}}_3\}$ oriented in any direction of the space.
- The control reference frame $\mathcal{R}$ defined as the frame where the control law is pointing to.
- The $j-$th thruster's reference frame $\mathcal{M}_j$ defined to have its origin in the N_j point and its first axis in the exhausting velocity direction $\boldsymbol{v}_{\mathrm{exh}_j}$.

Finally the instantaneous satellite's center of mass will be named C, the hub's center of mass will be labeled Bc/B and the $i-$th tank's center of mass will be noted Fc_i.

3 Mathematical Background

In this section the main tool used for the deduction of the governing equation will be presented and explained. The following theorem has always been called in the literature "Reynolds transport theorem" even if its first proof was given by Leibniz. The theorem provides a basic tool to pass from a Lagrangian formulation, based on the analysis of particles moving in space, to an Eulerian one, which considers a fixed space volume where physical quantities are exchanged throughout the boundaries.

In the present document the considered Lagrangian system will be labeled

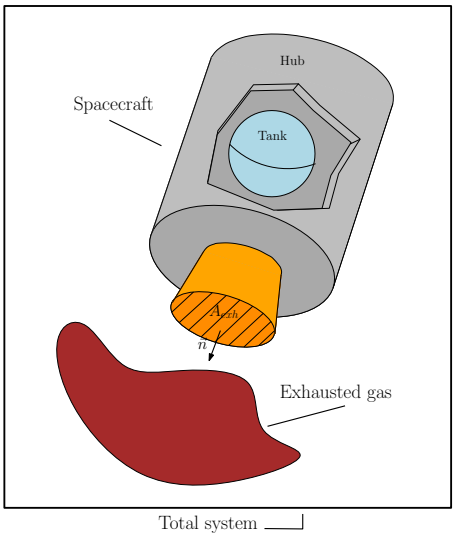

Figure 1: Division of the total system in spacecraft and exhausted gas. The control surface $\mathcal{A}_{\text{sc}}$ represents the exchanging surface between the two subsystems.

Body, the moving volume of the Eulerian approach will be called $\mathcal{V}_{\text{sc}}$ and its surface $\mathcal{A}_{\text{sc}}$. By using this notation, the theorem affirms [1, 2, 3, 4]:

$$\frac{\mathrm{d}}{\mathrm{d}t}\int_{Body}\rho\,\boldsymbol{f}\mathrm{d}\mathcal{V}=\frac{\mathrm{d}}{\mathrm{d}\,t}\int_{\mathcal{V}}\rho\,\boldsymbol{f}\mathrm{d}\mathcal{V}+\int_{\mathcal{A}}\rho\,\boldsymbol{f}\,(\boldsymbol{v}_{\text{rel}}\cdot\hat{\boldsymbol{n}})\,\mathrm{d}A \tag{1}$$

where $\boldsymbol{f}$ is a general vectorial quantity transported out from the control volume, ρ is the density of the infinitesimal mass $\mathrm{d}m$, $\hat{\boldsymbol{n}}$ the surface normal considered positive if exiting from the control volume and $\boldsymbol{v}_{\text{rel}}$ is the relative velocity of the particles flowing out from the surface with respect to the control surface itself. Moreover, in the case of a non deforming control surface, the following relation can be proved [2, 5] as no modification of the volume occurs:

$$\frac{\mathrm{d}}{\mathrm{d}\,t}\int_{Body}\rho\,\boldsymbol{f}\mathrm{d}\mathcal{V}=\int_{\mathcal{V}}\frac{\mathrm{d}}{\mathrm{d}\,t}\,(\rho\,\boldsymbol{f})\,\mathrm{d}\mathcal{V}+\int_{\mathcal{A}}\rho\,\boldsymbol{f}\,(\boldsymbol{v}_{\text{rel}}\cdot\hat{\boldsymbol{n}})\,\mathrm{d}A \tag{2}$$

4 Equation of motion

4.1 Translational equation

The inference of translational equation must begin considering the Newton's law for a closed system.

$$\frac{^{\mathcal{N}}\mathrm{d}}{\mathrm{d}\,t}\int_{Body}\dot{\boldsymbol{r}}_{M/N}\,\mathrm{d}m=\boldsymbol{F}_{\mathrm{ext}} \tag{3}$$

where $\dot{\boldsymbol{r}}_{M/N}$ is the velocity of the particle at the M point expressed in the inertial reference frame and $\boldsymbol{F}_{ext}$ are the external forces experienced by the body.
As the mass system is constant, the differentiation operator can be brought inside the integration and the use the kinematics equations allow to pass from the inertial reference frame $\mathcal{N}$ to the rotating and non-inertial $\mathcal{B}$:

$$\frac{^{\mathcal{N}}\mathrm{d}}{\mathrm{d}\,t}\int_{Body}\dot{\boldsymbol{r}}_{M/N}\,\mathrm{d}m=\int_{Body}\ddot{\boldsymbol{r}}_{M/N}\,\mathrm{d}m \tag{4}$$

The acceleration of the origin of the $\mathcal{B}$ frame can be expressed as:

$$\ddot{\boldsymbol{r}}_{M/N}=\ddot{\boldsymbol{r}}_{B/N}+\ddot{\boldsymbol{r}}_{M/B} \tag{5}$$

By using the kinematic transport theorem, the expression of $\boldsymbol{r}$ can be deduced:

$$\dot{\boldsymbol{r}}_{M/B}=\boldsymbol{r}'_{M/B}+\boldsymbol{\omega}_{\mathcal{B}/\mathcal{N}}\times\boldsymbol{r}_{M/B} \tag{6}$$

$$\ddot{\boldsymbol{r}}_{M/B}=\boldsymbol{r}''_{M/B}+2\,\boldsymbol{\omega}_{\mathcal{B}/\mathcal{N}}\times\boldsymbol{r}'_{M/B}+\dot{\boldsymbol{\omega}}_{\mathcal{B}/\mathcal{N}}\times\boldsymbol{r}_{M/B}+\boldsymbol{\omega}_{\mathcal{B}/\mathcal{N}}\times\left(\boldsymbol{\omega}_{\mathcal{B}/\mathcal{N}}\times\boldsymbol{r}_{B/M}\right) \tag{7}$$

A Lagrangian formulation of the linear momentum equation can be deduced by using equations 3, 4, 5 and 7:

$$\begin{aligned}\int_{Body}\left(\ddot{\boldsymbol{r}}_{B/N}+\dot{\boldsymbol{\omega}}_{\mathcal{B}/\mathcal{N}}\times\boldsymbol{r}_{M/B}+\boldsymbol{\omega}_{\mathcal{B}/\mathcal{N}}\times\left(\boldsymbol{\omega}_{\mathcal{B}/\mathcal{N}}\times\boldsymbol{r}_{M/B}\right)\right)\mathrm{d}m+\\ +2\,\boldsymbol{\omega}_{\mathcal{B}/\mathcal{N}}\times\int_{Body}\boldsymbol{r}'_{M/B}\mathrm{d}m+\int_{Body}\boldsymbol{r}''_{M/B}\mathrm{d}m=\boldsymbol{F}_{\mathrm{ext}}\end{aligned} \tag{8}$$

As the system mass is constant, the derivation operator can be applied after the integration. Thus:

$$\int_{Body}\boldsymbol{r}'_{M/B}\mathrm{d}m=\frac{^{\mathcal{B}}\mathrm{d}}{\mathrm{d}t}\int_{Body}\boldsymbol{r}_{M/B}\mathrm{d}m \tag{9}$$

$$\int_{Body}\boldsymbol{r}''_{M/B}\mathrm{d}m=\frac{^{\mathcal{B}}\mathrm{d}^2}{\mathrm{d}t^2}\int_{Body}\boldsymbol{r}_{M/B}\mathrm{d}m \tag{10}$$

By using the Reynolds transport theorem,the two previous equations can be expressed in a space fixed volume, shown in figure 1.

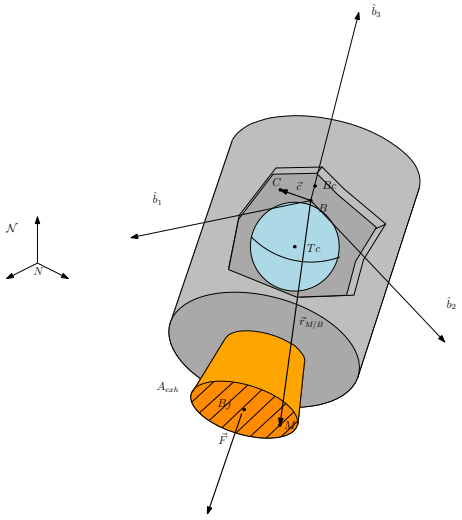

Figure 2: Spacecraft subsystem and main definitions.

$$\frac{{}^{\mathcal{B}}\mathrm{d}}{\mathrm{d}t}\int_{Body}\boldsymbol{r}_{M/B}\,\mathrm{d}m=\frac{{}^{\mathcal{B}}\mathrm{d}}{\mathrm{d}t}\int_{\mathcal{V}_{\mathrm{sc}}}\rho\,\boldsymbol{r}_{M/B}\,\mathrm{d}\mathcal{V}+\int_{\mathcal{A}_{\mathrm{sc}}}\rho\,\boldsymbol{r}'_{M/B}\cdot\hat{\boldsymbol{n}}\,\boldsymbol{r}_{M/B}\mathrm{d}A \tag{11}$$

$$\begin{aligned}\frac{{}^{\mathcal{B}}\mathrm{d}^2}{\mathrm{d}t^2}\int_{Body}\boldsymbol{r}_{M/B}\,\mathrm{d}m=&\frac{{}^{\mathcal{B}}\mathrm{d}^2}{\mathrm{d}t^2}\int_{\mathcal{V}_{\mathrm{sc}}}\rho\,\boldsymbol{r}_{M/B}\,\mathrm{d}\mathcal{V}+\\&+\frac{{}^{\mathcal{B}}\mathrm{d}}{\mathrm{d}t}\int_{\mathcal{A}_{\mathrm{sc}}}\rho\,\boldsymbol{r}'_{M/B}\cdot\hat{\boldsymbol{n}}\,\boldsymbol{r}_{M/B}\,\mathrm{d}A+\int_{\mathcal{A}_{\mathrm{sc}}}\rho\,\boldsymbol{r}'_{M/B}\cdot\hat{\boldsymbol{n}}\,\boldsymbol{r}'_{M/B}\,\mathrm{d}A\end{aligned} \tag{12}$$

where $\boldsymbol{v}_{\mathrm{rel}}=\boldsymbol{r}'_{M/B}$ because the B point is fixed with respect to the spacecraft and, clearly, the relative velocity of the particle in M is the the derivative of the position vector in the $\mathcal{B}$ reference frame.
The equation 8 can be re-organized by using the previous relations in order to consider an Eulerian approach, i.e. based on a volume-based view.

$$\begin{aligned}&\int_{Body}\left(\ddot{\boldsymbol{r}}_{B/N}+\dot{\boldsymbol{\omega}}_{\mathcal{B}/\mathcal{N}}\times\boldsymbol{r}_{M/B}+\boldsymbol{\omega}_{\mathcal{B}/\mathcal{N}}\times\left(\boldsymbol{\omega}_{\mathcal{B}/\mathcal{N}}\times\boldsymbol{r}_{M/B}\right)\right)\mathrm{d}m+\\&\quad+2\,\boldsymbol{\omega}_{\mathcal{B}/\mathcal{N}}\times\left(\frac{{}^{\mathcal{B}}\mathrm{d}}{\mathrm{d}t}\int_{\mathcal{V}_{\mathrm{sc}}}\rho\,\boldsymbol{r}_{M/B}\,\mathrm{d}\mathcal{V}+\int_{\mathcal{A}_{\mathrm{sc}}}\rho\,\boldsymbol{r}'_{M/B}\cdot\hat{\boldsymbol{n}}\,\boldsymbol{r}_{M/B}\mathrm{d}A\right)+\\&\quad+\frac{{}^{\mathcal{B}}\mathrm{d}^2}{\mathrm{d}t^2}\int_{\mathcal{V}_{\mathrm{sc}}}\rho\,\boldsymbol{r}_{M/B}\,\mathrm{d}\mathcal{V}+\frac{{}^{\mathcal{B}}\mathrm{d}}{\mathrm{d}t}\int_{\mathcal{A}_{\mathrm{sc}}}\rho\,\boldsymbol{r}'_{M/B}\cdot\hat{\boldsymbol{n}}\,\boldsymbol{r}_{M/B}\,\mathrm{d}A+\\&\quad+\int_{\mathcal{A}_{\mathrm{sc}}}\rho\,\boldsymbol{r}'_{M/B}\cdot\hat{\boldsymbol{n}}\,\boldsymbol{r}'_{M/B}\,\mathrm{d}A=\boldsymbol{F}_{\mathrm{ext}}\end{aligned} \tag{13}$$

As explained in [1], if at the initial time all the mass is contained in the control volume a particular relation stands as no mass is outside the volume of control at $t = 0$ and the dynamic quantities will be transported out by the fluxes during the integration:

$$\begin{aligned}\boldsymbol{F}_{\text{ext}} - \int_{Body} \left(\ddot{\boldsymbol{r}}_{B/N} + \dot{\boldsymbol{\omega}}_{\mathcal{B}/\mathcal{N}} \times \boldsymbol{r}_{M/B} + \boldsymbol{\omega}_{\mathcal{B}/\mathcal{N}} \times \left(\boldsymbol{\omega}_{\mathcal{B}/\mathcal{N}} \times \boldsymbol{r}_{M/B}\right)\right) \mathrm{d}m = \\ = \int_{\mathcal{V}_{\text{sc}}} \mathrm{d}\boldsymbol{F}_{\text{vol}} + \int_{\mathcal{A}_{\text{sc}}} \mathrm{d}\boldsymbol{F}_{\text{surf}} - \int_{\mathcal{V}_{\text{sc}}} \rho \left(\ddot{\boldsymbol{r}}_{B/N} + \dot{\boldsymbol{\omega}}_{\mathcal{B}/\mathcal{N}} \times \boldsymbol{r}_{M/B} + \right. \\ \left. + \boldsymbol{\omega}_{\mathcal{B}/\mathcal{N}} \times \left(\boldsymbol{\omega}_{\mathcal{B}/\mathcal{N}} \times \boldsymbol{r}_{M/B}\right)\right) \mathrm{d}\mathcal{V} \quad (14)\end{aligned}$$

where the forces has been divided on the volumetric ones and the ones applied on the spacecraft surface.
Thus:

$$\begin{aligned}\int_{\mathcal{V}_{\text{sc}}} \rho \left(\ddot{\boldsymbol{r}}_{B/N} + \dot{\boldsymbol{\omega}}_{\mathcal{B}/\mathcal{N}} \times \boldsymbol{r}_{M/B} + \boldsymbol{\omega}_{\mathcal{B}/\mathcal{N}} \times \left(\boldsymbol{\omega}_{\mathcal{B}/\mathcal{N}} \times \boldsymbol{r}_{M/B}\right)\right) \mathrm{d}\mathcal{V} + \\ + 2\,\boldsymbol{\omega}_{\mathcal{B}/\mathcal{N}} \times \left(\frac{{}^{\mathcal{B}}\mathrm{d}}{\mathrm{d}t} \int_{\mathcal{V}_{\text{sc}}} \rho\, \boldsymbol{r}_{M/B}\, \mathrm{d}\mathcal{V} + \int_{\mathcal{A}_{\text{sc}}} \rho\, \boldsymbol{r}'_{M/B} \cdot \hat{\boldsymbol{n}}\, \boldsymbol{r}_{M/B} \mathrm{d}A\right) + \\ + \frac{{}^{\mathcal{B}}\mathrm{d}^2}{\mathrm{d}t^2} \int_{\mathcal{V}_{\text{sc}}} \rho\, \boldsymbol{r}_{M/B}\, \mathrm{d}\mathcal{V} + \frac{{}^{\mathcal{B}}\mathrm{d}}{\mathrm{d}t} \int_{\mathcal{A}_{\text{sc}}} \rho\, \boldsymbol{r}'_{M/B} \cdot \hat{\boldsymbol{n}}\, \boldsymbol{r}_{M/B}\, \mathrm{d}A + \\ + \int_{\mathcal{A}_{\text{sc}}} \rho\, \boldsymbol{r}'_{M/B} \cdot \hat{\boldsymbol{n}}\, \boldsymbol{r}'_{M/B}\, \mathrm{d}A = \int_{\mathcal{V}_{\text{sc}}} \mathrm{d}\boldsymbol{F}_{\text{vol}} + \int_{\mathcal{A}_{\text{sc}}} \mathrm{d}\boldsymbol{F}_{\text{surf}} \quad (15)\end{aligned}$$

As the present paper aims to introduce the dynamic equations in case of varying mass inside the spacecraft, two point must be developed: on the one hand both the translational equation and the rotational one will be expressed with the vector $\boldsymbol{r}_{B/N}$ as free variable and, on the other, a complete and comprehensive model of the $\boldsymbol{c} = \boldsymbol{r}_{C/B}$ vector must be performed in order to follow the instantaneous displacement of the center of mass all along the trajectory of the satellite.
Calculating the satellite's center of mass in the $\mathcal{B}$ reference frame, the $\boldsymbol{c}$ vector can be expressed with respect to the mass of each spacecraft component.

$$\boldsymbol{c} = \frac{m_{\text{hub}}\, \boldsymbol{r}_{Bc/B} + \sum_{i=1}^{M} m_{\text{fuel}_i}\, \boldsymbol{r}_{Fc_i/B}}{m_{\text{hub}} + \sum_{i=1}^{M} m_{\text{fuel}_i}} \quad (16)$$

where m_{hub} is the hub mass, m_{fuel_i} the i-th fuel mass and $\boldsymbol{r}_{Fc_i/B}$ the position of the i-th fuel's center of mass.
In order to infer the influence of the mass variation in the equation of motion the relation 16 must be derived. Thus, in the $\mathcal{B}$ frame:

$$\boldsymbol{c}' = \frac{\sum_{i=1}^{M}\left(\dot{m}_{\text{fuel}_i}\boldsymbol{r}_{Fc_i/B} + m_{\text{fuel}_i}\boldsymbol{r}'_{Fc_i/B}\right)}{m_{\text{hub}} + \sum_{i=1}^{M} m_{\text{fuel}_i}} + \\ - \frac{\left(\sum_{i=1}^{M}\dot{m}_{\text{fuel}_i}\right)\left(m_{\text{hub}}\,\boldsymbol{r}_{Bc/B} + \sum_{i=1}^{M} m_{\text{fuel}_i}\,\boldsymbol{r}_{Fc_i/B}\right)}{\left(m_{\text{hub}} + \sum_{i=1}^{M} m_{\text{fuel}_i}\right)^2} \tag{17}$$

$$\boldsymbol{c}'' = \frac{\sum_{i=1}^{M}\left(\ddot{m}_{\text{fuel}_i}\boldsymbol{r}_{Fc_i/B} + 2\,\dot{m}_{\text{fuel}_i}\boldsymbol{r}'_{Fc_i/B} + m_{\text{fuel}_i}\boldsymbol{r}''_{Fc_i/B}\right)}{m_{\text{hub}} + \sum_{i=1}^{M} m_{\text{fuel}_i}} + \\ - \frac{\left(\sum_{i=1}^{M}\ddot{m}_{\text{fuel}_i}\right)\left(m_{\text{hub}}\,\boldsymbol{r}_{Bc/B} + \sum_{i=1}^{M} m_{\text{fuel}_i}\,\boldsymbol{r}_{Fc_i/B}\right)}{\left(m_{\text{hub}} + \sum_{i=1}^{M} m_{\text{fuel}_i}\right)^2} + \\ - \frac{2\left(\sum_{i=1}^{M}\dot{m}_{\text{fuel}_i}\right)\sum_{i=1}^{M}\left(\dot{m}_{\text{fuel}_i}\boldsymbol{r}_{Fc_i/B} + m_{\text{fuel}_i}\boldsymbol{r}'_{Fc_i/B}\right)}{\left(m_{\text{hub}} + \sum_{i=1}^{M} m_{\text{fuel}_i}\right)^2} + \\ + \frac{2\left(\sum_{i=1}^{M}\dot{m}_{\text{fuel}_i}\right)^2\left(m_{\text{hub}}\boldsymbol{r}_{Bc/B} + \sum_{i=1}^{M} m_{\text{fuel}_i}\boldsymbol{r}_{Fc_i/B}\right)}{\left(m_{\text{hub}} + \sum_{i=1}^{M} m_{\text{fuel}_i}\right)^3} \tag{18}$$

Once the vector $\boldsymbol{c}$ has been evaluated, the completed translational equation of motion can be simplified both assuming no relative internal mass flow inside the reference volume and expressing each term with respect to nozzle's position and geometric feature of each thruster.
In the following pages the terms of equation 15 will be analyzed in order to have a simpler relation adapted to the case under study. The main hypothesis that will be taken into account are:

- The body is rigid and deformations are not considered.
- The mass flow among the tanks and the thrusters is considered to be a second order effect and, thus, neglected.
- The particles are accelerated instantaneously from the spacecraft velocity $\dot{\boldsymbol{r}}_{B/N}$ to the exhausted velocity $\boldsymbol{v}_{\text{exh}}$ at the nozzle exit.
- The particle exhausted velocity $\boldsymbol{v}_{\text{exh}}$ is considered constant and parallel to the nozzle's normal $\hat{\boldsymbol{n}}$

The first integral in equation 15 is the easiest to compute by tanking into account that $\boldsymbol{r}_{M/B} = \boldsymbol{c} + \boldsymbol{r}_{M/C}$ and the definition of barycenter:

$$\int_{\mathcal{V}_{\rm sc}} \rho \left(\ddot{\boldsymbol{r}}_{B/N} + \dot{\boldsymbol{\omega}}_{\mathcal{B}/\mathcal{N}} \times \boldsymbol{r}_{M/B} + \boldsymbol{\omega}_{\mathcal{B}/\mathcal{N}} \times \left(\boldsymbol{\omega}_{\mathcal{B}/\mathcal{N}} \times \boldsymbol{r}_{M/B} \right) \right) \mathrm{d}\mathcal{V} =$$
$$= m_{\rm sc}\, \ddot{\boldsymbol{r}}_{B/N} + m_{\rm sc}\, \dot{\boldsymbol{\omega}}_{\mathcal{B}/\mathcal{N}} \times \boldsymbol{c} + m_{\rm sc}\, \boldsymbol{\omega}_{\mathcal{B}/\mathcal{N}} \times \left(\boldsymbol{\omega}_{\mathcal{B}/\mathcal{N}} \times \boldsymbol{c} \right) \quad (19)$$

where $m_{\rm sc} = m_{\rm hub} + \sum_{i=1}^{M} m_{{\rm fuel}_i}$ is the instantaneous mass of the spacecraft. As far as the second and the forth integral concern, their expression can be gathered throughout the definition of barycenter and the kinematic decomposition of the vector $\boldsymbol{r}_{M/B}$. Thus:

$$\frac{^{\mathcal{B}}\mathrm{d}}{\mathrm{d}t} \int_{\mathcal{V}_{\rm sc}} \rho\, \boldsymbol{r}_{M/B}\, \mathrm{d}\mathcal{V} = \frac{^{\mathcal{B}}\mathrm{d}}{\mathrm{d}t} \left(m_{\rm sc}\, \boldsymbol{c} \right) = m_{\rm sc}\, \boldsymbol{c}' + \dot{m}_{\rm fuel} \boldsymbol{c} \quad (20)$$

where $\dot{m}_{\rm fuel} = \sum_{i=1}^{M} \dot{m}_{{\rm fuel}_i}$.

$$\frac{^{\mathcal{B}}\mathrm{d}^2}{\mathrm{d}t^2} \int_{\mathcal{V}_{\rm sc}} \rho\, \boldsymbol{r}_{M/B}\, \mathrm{d}\mathcal{V} = \frac{^{\mathcal{B}}\mathrm{d}^2}{\mathrm{d}t^2} \left(m_{\rm sc}\, \boldsymbol{c} \right) = m_{\rm sc}\, \boldsymbol{c}'' + 2\, \dot{m}_{\rm fuel}\, \boldsymbol{c}' + \ddot{m}_{\rm fuel} \boldsymbol{c} \quad (21)$$

where $\ddot{m}_{\rm fuel} = \sum_{i=1}^{M} \ddot{m}_{{\rm fuel}_i}$.
In order to infer the term calculated on the reference surface, i.e. the third, the fifth and the sixth integrals, it could be convenient to separate the integral on the surface of each nozzle and then sum them all. Moreover, as the fuel's properties are flowing out from a circular surface, it is convenient to express the vector $\boldsymbol{r}_{M/B}$ as follows $\boldsymbol{r}_{M/B} = \boldsymbol{r}_{M/Fc_j} + \boldsymbol{r}_{Fc_j/B}$ where Fc_i is the area's barycenter. Finally, a convenient variable transformation can be performed to compute the properties exchanged while the mass disk is passing through the reference surface, i.e. $\mathrm{d}\dot{m} = -\rho\, \boldsymbol{r}'_{M/B} \cdot \hat{\boldsymbol{n}} \mathrm{d}A$.

$$\int_{\mathcal{A}_{\rm sc}} \rho\, \boldsymbol{r}'_{M/B} \cdot \hat{\boldsymbol{n}}\, \boldsymbol{r}_{M/B}\, \mathrm{d}A = \sum_{j=1}^{N} \int_{\mathcal{A}_{{\rm noz}_j}} \rho\, \boldsymbol{r}'_{M/B} \cdot \boldsymbol{n}\, \boldsymbol{r}_{M/B}\, \mathrm{d}A =$$
$$= -\sum_{j=1}^{N} \int_{\dot{m}_{{\rm noz}_j}} \left(\boldsymbol{r}_{M/N_j} + \boldsymbol{r}_{N_j/B} \right) \mathrm{d}\dot{m} = -\sum_{j=1}^{N} \dot{m}_{{\rm noz}_j} \boldsymbol{r}_{N_j/B} \quad (22)$$

where the first part of the integral is null because of barycenter definition and $\dot{m}_{{\rm noz}_j}$ is the mass flow of the $j-$th nozzle.

$$\frac{^{\mathcal{B}}\mathrm{d}}{\mathrm{d}t} \int_{\mathcal{A}_{\rm sc}} \rho\, \boldsymbol{r}'_{M/B} \cdot \hat{\boldsymbol{n}}\, \boldsymbol{r}_{M/B}\, \mathrm{d}A = \frac{^{\mathcal{B}}\mathrm{d}}{\mathrm{d}t} \left(-\sum_{j=1}^{N} \dot{m}_{{\rm noz}_j} \boldsymbol{r}_{N_j/B} \right) =$$
$$= -\sum_{j=1}^{N} \left(\ddot{m}_{{\rm noz}_j} \boldsymbol{r}_{N_j/B} + \dot{m}_{{\rm noz}_j} \boldsymbol{r}'_{N_j/B} \right) = -\sum_{j=1}^{N} \ddot{m}_{{\rm noz}_j} \boldsymbol{r}_{N_j/B} \quad (23)$$

where the last equivalence stands as the nozzle barycenter is motionless with respect to the body-fixed point B and $\ddot{m}_{\mathrm{noz}_j}$ is the mass flow derivative of the $j-$th nozzle.
The sixth integral can be easily solved if the exhausted velocity $\boldsymbol{r}'_{M/B} = \boldsymbol{v}_{\mathrm{exh}}$ is considered constant at the nozzle's exit, as hypothesized previously.

$$\int_{\mathcal{A}_{\mathrm{sc}}} \rho\, \boldsymbol{r}'_{M/B} \cdot \hat{\boldsymbol{n}}\, \boldsymbol{r}'_{M/B}\, \mathrm{d}A = \sum_{j=1}^{N} \int_{\mathcal{A}_{\mathrm{noz}_j}} \rho\, \boldsymbol{r}'_{M/B} \cdot \boldsymbol{n}\, \boldsymbol{r}'_{M/B} \mathrm{d}A = \\ = -\sum_{j=1}^{N} \int_{\dot{m}_{\mathrm{noz}_j}} \boldsymbol{v}_{\mathrm{exh}}\, \mathrm{d}\dot{m} = -\sum_{j=1}^{N} \dot{m}_{\mathrm{noz}_j}\, \boldsymbol{v}_{\mathrm{exh}_j} \quad (24)$$

where $\boldsymbol{v}_{\mathrm{exh}_j}$ is the exhausted velocity of a particle exiting from the $j-$th nozzle.
Finally the two integrals of the right member of equation 15 can easily computed once a force model is chosen. This step depends directly from the problem under study. As the present work aims to provide general rotational and translational equations, the only term that can be developed analytically is the surfacing integral to take into account the effect of the pressure jump between the nozzle and the environment. Thus:

$$\int_{\mathcal{V}_{\mathrm{sc}}} \mathrm{d}\boldsymbol{F}_{\mathrm{vol}} + \int_{\mathcal{A}_{\mathrm{sc}}} \mathrm{d}\boldsymbol{F}_{\mathrm{surf}} = \boldsymbol{F}_{\mathrm{ext,\ vol}} + \boldsymbol{F}_{\mathrm{ext,\ surf}} + \\ + \sum_{j=1}^{N} \frac{\boldsymbol{v}_{\mathrm{exh}_j}}{v_{\mathrm{exh}_j}} A_{\mathrm{noz}_j} \left(p_{\mathrm{exh}_j} - p_{\mathrm{atm}}\right) \quad (25)$$

where $\boldsymbol{F}_{\mathrm{ext,\ vol}}$ are the external forces acting on the control volume, $\boldsymbol{F}_{\mathrm{ext,\ surf}}$ are the external forces accelerating the control surface, p_{exh_j} is the particles' exhausted pressure at the $j-$th nozzle and p_{atm} is the atmospheric pressure at the flying altitude.
Finally, the equation 15 can be rewritten considering nozzles' geometry and fluid properties by using equations 20, 21, 22, 23, 24, 25.

$$m_{\mathrm{sc}} \ddot{\boldsymbol{r}}_{B/N} + m_{\mathrm{sc}}\, \dot{\boldsymbol{\omega}}_{\mathcal{B}/\mathcal{N}} \times \boldsymbol{c} + m_{\mathrm{sc}}\, \boldsymbol{\omega}_{\mathcal{B}/\mathcal{N}} \times \left(\boldsymbol{\omega}_{\mathcal{B}/\mathcal{N}} \times \boldsymbol{c}\right) + m_{\mathrm{sc}}\, \boldsymbol{c}'' + 2\, \dot{m}_{\mathrm{fuel}}\, \boldsymbol{c}' + \\ + \ddot{m}_{\mathrm{fuel}} \boldsymbol{c} + 2\, \boldsymbol{\omega}_{\mathcal{B}/\mathcal{N}} \times \left(m_{\mathrm{sc}}\, \boldsymbol{c}' + \dot{m}_{\mathrm{fuel}} \boldsymbol{c} - \sum_{j=1}^{N} \dot{m}_{\mathrm{noz}_j} \boldsymbol{r}_{N_j/B}\right) - \sum_{j=1}^{N} \ddot{m}_{\mathrm{noz}_j} \boldsymbol{r}_{N_j/B} + \\ - \sum_{j=1}^{N} \dot{m}_{\mathrm{noz}_j}\, \boldsymbol{v}_{\mathrm{exh}_j} = \boldsymbol{F}_{\mathrm{ext,\ vol}} + \boldsymbol{F}_{\mathrm{ext,\ surf}} + \sum_{j=1}^{N} \frac{\boldsymbol{v}_{\mathrm{exh}_j}}{v_{\mathrm{exh}_j}} A_{\mathrm{noz}_j} \left(p_{\mathrm{exh}_j} - p_{\mathrm{atm}}\right) \quad (26)$$

where $\boldsymbol{c}$, $\boldsymbol{c}'$, $\boldsymbol{c}''$ have been specified in equations 16, 18, 19.
The previous equation can be righted by defining the following quantity:

$$\boldsymbol{F}_{\mathrm{thr}_j} = \boldsymbol{v}_{\mathrm{exh}_j} \left(\frac{A_{\mathrm{noz}_j}}{v_{\mathrm{exh}_j}} \left(p_{\mathrm{exh}_j} - p_{\mathrm{atm}} \right) + \dot{m}_{\mathrm{noz}_j} \right) = I_{\mathrm{sp}_j} \, g_0 \, \dot{m}_{\mathrm{noz}_j} \frac{\boldsymbol{v}_{\mathrm{exh}_j}}{v_{\mathrm{exh}_j}} \tag{27}$$

Thus:

$$\begin{aligned} \ddot{\boldsymbol{r}}_{B/N} - \boldsymbol{c} \times \dot{\boldsymbol{\omega}}_{\mathcal{B}/\mathcal{N}} = &+ \frac{1}{m_{\mathrm{sc}}} \sum_{j=1}^{N} \boldsymbol{F}_{\mathrm{thr}_j} - 2 \, \frac{\dot{m}_{\mathrm{fuel}}}{m_{\mathrm{sc}}} \left(\boldsymbol{c}' + \boldsymbol{\omega}_{\mathcal{B}/\mathcal{N}} \times \boldsymbol{c} \right) - \boldsymbol{c}'' + \\ &- 2 \, \boldsymbol{\omega}_{\mathcal{B}/\mathcal{N}} \times \boldsymbol{c}' - \boldsymbol{\omega}_{\mathcal{B}/\mathcal{N}} \times \left(\boldsymbol{\omega}_{\mathcal{B}/\mathcal{N}} \times \boldsymbol{c} \right) + \frac{2}{m_{\mathrm{sc}}} \sum_{j=1}^{N} \dot{m}_{\mathrm{noz}_j} \boldsymbol{\omega}_{\mathcal{B}/\mathcal{N}} \times \boldsymbol{r}_{N_j/B} + \\ &+ \frac{1}{m_{\mathrm{sc}}} \sum_{j=1}^{N} \ddot{m}_{\mathrm{noz}_j} \boldsymbol{r}_{N_j/B} - \ddot{m}_{\mathrm{fuel}} \, \boldsymbol{c} + \frac{1}{m_{\mathrm{sc}}} \boldsymbol{F}_{\mathrm{ext,\ vol}} + \frac{1}{m_{\mathrm{sc}}} \boldsymbol{F}_{\mathrm{ext,\ surf}} \end{aligned} \tag{28}$$

Moreover, if the cross product is substituted with the associated skew matrix, the translational equation 28 can be written in a more compact form:

$$\begin{aligned} \ddot{\boldsymbol{r}}_{B/N} + \left[\tilde{\boldsymbol{c}} \right]^T \dot{\boldsymbol{\omega}}_{\mathcal{B}/\mathcal{N}} = &+ \frac{1}{m_{\mathrm{sc}}} \sum_{j=1}^{N} \boldsymbol{F}_{\mathrm{thr}_j} - 2 \, \frac{\dot{m}_{\mathrm{fuel}}}{m_{\mathrm{sc}}} \left(\boldsymbol{c}' + \left[\tilde{\boldsymbol{\omega}}_{\mathcal{B}/\mathcal{N}} \right] \times \boldsymbol{c} \right) - \boldsymbol{c}'' + \\ &+ 2 \left[\tilde{\boldsymbol{\omega}}_{\mathcal{B}/\mathcal{N}} \right]^T \boldsymbol{c}' + \left[\tilde{\boldsymbol{\omega}}_{\mathcal{B}/\mathcal{N}} \right]^T \left[\tilde{\boldsymbol{\omega}}_{\mathcal{B}/\mathcal{N}} \right] \boldsymbol{c} + \frac{2}{m_{\mathrm{sc}}} \sum_{j=1}^{N} \dot{m}_{\mathrm{noz}_j} \left[\tilde{\boldsymbol{\omega}}_{\mathcal{B}/\mathcal{N}} \right] \boldsymbol{r}_{N_j/B} + \\ &+ \frac{1}{m_{\mathrm{sc}}} \sum_{j=1}^{N} \ddot{m}_{\mathrm{noz}_j} \boldsymbol{r}_{Fc_j/B} - \ddot{m}_{\mathrm{fuel}} \, \boldsymbol{c} + \frac{1}{m_{\mathrm{sc}}} \boldsymbol{F}_{\mathrm{ext,\ vol}} + \frac{1}{m_{\mathrm{sc}}} \boldsymbol{F}_{\mathrm{ext,\ surf}} \end{aligned} \tag{29}$$

This equation of motion is the Newton's law for an open system subjected to external forces $\boldsymbol{F}_{\mathrm{ext,\ vol}} + \boldsymbol{F}_{\mathrm{ext,\ surf}}$ and thrust $\boldsymbol{F}_{\mathrm{thr}} = \sum_{j=1}^{N} \boldsymbol{F}_{\mathrm{thr}_j}$ due to mass depletion of the spacecraft, represented in figure 2. From this equation it can be deduced that the variation of the mass inside the spacecraft affects directly the position of the satellite with respect to the origin as the body fixed point B changes its state of motion according to the variation of the tanks' linear inertia.

4.2 Rotational Motion

In this section the rotational equation of motion will be developed taking into account the variation of fuel in the reservoirs. Beginning from the Newton's equation and calling M the point where the infinitesimal mass $\mathrm{d}m$ is:

$$\ddot{\boldsymbol{r}}_{M/N} \, \mathrm{d}m = \mathrm{d}\boldsymbol{F} \quad \Rightarrow \quad \boldsymbol{r}_{M/N} \times \ddot{\boldsymbol{r}}_{M/N} \, \mathrm{d}m = \boldsymbol{r}_{M/N} \times \mathrm{d}\boldsymbol{F} \tag{30}$$

By performing an integration allover the system:

$$\int_{Body} \boldsymbol{r}_{M/N} \times \ddot{\boldsymbol{r}}_{M/N} \, \mathrm{d}m = \int_{Body} \boldsymbol{r}_{M/N} \times \mathrm{d}\boldsymbol{F} \tag{31}$$

The left term of the equation can be manipulated in order to consider a different reference of the origin of the momentum equation thanks to kinematics identities:

$$\begin{aligned} &\int_{Body} \rho \, \boldsymbol{r}_{M/N} \times \ddot{\boldsymbol{r}}_{M/N} \, \mathrm{d}\mathcal{V} = \int_{Body} \rho \, \boldsymbol{r}_{M/B} \times \ddot{\boldsymbol{r}}_{M/B} \, \mathrm{d}\mathcal{V} + \\ &+ \int_{Body} \rho \, \boldsymbol{r}_{B/N} \times \ddot{\boldsymbol{r}}_{M/N} \, \mathrm{d}\mathcal{V} + \int_{Body} \rho \, \boldsymbol{r}_{M/B} \times \ddot{\boldsymbol{r}}_{B/N} \, \mathrm{d}\mathcal{V} = \int_{Body} \boldsymbol{r}_{M/N} \times \mathrm{d}\boldsymbol{F} \end{aligned} \tag{32}$$

Considering that $\ddot{\boldsymbol{r}}_{M/N} \, \mathrm{d}m = \mathrm{d}\boldsymbol{F}$, the torque caused by the forces acting on the body can be easily defined:

$$\begin{aligned} &\int_{Body} \boldsymbol{r}_{M/N} \times \mathrm{d}\boldsymbol{F} - \int_{Body} \rho \, \boldsymbol{r}_{B/N} \times \ddot{\boldsymbol{r}}_{M/N} \, \mathrm{d}\mathcal{V} = \\ &\qquad = \int_{Body} \left(\boldsymbol{r}_{M/N} - \boldsymbol{r}_{B/N} \right) \times \mathrm{d}\boldsymbol{F} = \int_{Body} \boldsymbol{r}_{M/B} \times \mathrm{d}\boldsymbol{F} = \boldsymbol{L}_B \end{aligned} \tag{33}$$

where $\boldsymbol{L}_B$ is the torque with respect to the body-fixed point B.
As the mass of the system is constant, the derivative of the angular momentum about point B can be inferred easily from equation 32 thanks to the property of the cross product and the previously exposed Reynold transport theorem:

$$\begin{aligned} \int_{Body} \rho \, \boldsymbol{r}_{M/B} \times \ddot{\boldsymbol{r}}_{M/B} \, \mathrm{d}\mathcal{V} = \frac{{}^{\mathcal{N}}\mathrm{d}}{\mathrm{d}t} \int_{\mathcal{V}_{\mathrm{sc}}} \rho \, \boldsymbol{r}_{M/B} \times \dot{\boldsymbol{r}}_{M/B} \, \mathrm{d}\mathcal{V} + \\ + \int_{\mathcal{A}_{\mathrm{sc}}} \rho \, \boldsymbol{r}'_{M/B} \cdot \hat{\boldsymbol{n}} \left(\boldsymbol{r}_{M/B} \times \dot{\boldsymbol{r}}_{M/B} \right) \mathrm{d}A \end{aligned} \tag{34}$$

Moreover, as in the translational equation, if all the mass of the system is contained at the initial time inside the control volume, the following relation stands:

$$\begin{aligned} \int_{Body} \rho \, \boldsymbol{r}_{M/B} \times \ddot{\boldsymbol{r}}_{B/N} \, \mathrm{d}\mathcal{V} - \boldsymbol{L}_B = \int_{\mathcal{V}_{\mathrm{sc}}} \rho \, \boldsymbol{r}_{M/B} \times \ddot{\boldsymbol{r}}_{B/N} \, \mathrm{d}\mathcal{V} - \int_{\mathcal{V}_{\mathrm{sc}}} \boldsymbol{r}_{M/B} \times \mathrm{d}\boldsymbol{F}_{\mathrm{vol}} + \\ - \int_{\mathcal{A}_{\mathrm{sc}}} \boldsymbol{r}_{M/B} \times \mathrm{d}\boldsymbol{F}_{\mathrm{surf}} = m_{\mathrm{sc}} \boldsymbol{c} \times \ddot{\boldsymbol{r}}_{B/N} - \boldsymbol{L}_{B,\,\mathrm{vol}} - \boldsymbol{L}_{B,\,\mathrm{surf}} \end{aligned} \tag{35}$$

where $\boldsymbol{L}_{B,\,\mathrm{vol}}$ and $\boldsymbol{L}_{B,\,\mathrm{surf}}$ are the torques caused by the volume forces and surface one respectively.

Finally, the general rotational equation for a control volume in a rotating reference frame can be reorganized:

$$\dot{\boldsymbol{H}}_{\mathrm{sc},\,B} + \int_{\mathcal{A}_{\mathrm{sc}}} \rho\, \boldsymbol{r}'_{M/B} \cdot \hat{\boldsymbol{n}} \left(\boldsymbol{r}_{M/B} \times \dot{\boldsymbol{r}}_{M/B}\right) \mathrm{d}A + m_{\mathrm{sc}} \boldsymbol{c} \times \ddot{\boldsymbol{r}}_{B/N} = \\ = \boldsymbol{L}_{B,\,\mathrm{vol}} + \boldsymbol{L}_{B,\,\mathrm{surf}} \quad (36)$$

By definition of angular momentum vector about point B:

$$\boldsymbol{H}_{\mathrm{sc},\,B} = [I_{\mathrm{hub},\,Bc}]\, \boldsymbol{\omega}_{\mathcal{B}/\mathcal{N}} + \boldsymbol{r}_{Bc/B} \times m_{\mathrm{hub}}\, \dot{\boldsymbol{r}}_{Bc/B} + \\ + \sum_{i=1}^{M} \left([I_{\mathrm{fuel}_i,\,Fc_i}]\, \boldsymbol{\omega}_{\mathcal{B}/\mathcal{N}} + \boldsymbol{r}_{Fc_i/B} \times m_{\mathrm{fuel}_i}\, \dot{\boldsymbol{r}}_{Fc_i/B}\right) \quad (37)$$

where $[I_{\mathrm{hub},\,Bc}]$ is the hub's inertia about its center of mass Bc and $[I_{\mathrm{fuel}_i,\,Fc_i}]$ is the $i-$th tank's inertia about its center of mass Fc_i.
Furthermore, an analytical expression of mass depletion on the rotational motion can be deduced:

$$\dot{\boldsymbol{H}}_{\mathrm{sc},\,B} = [I_{\mathrm{hub},\,Bc}]\, \dot{\boldsymbol{\omega}}_{\mathcal{B}/\mathcal{N}} + \boldsymbol{\omega}_{\mathcal{B}/\mathcal{N}} \times \left([I_{\mathrm{hub},\,Bc}]\, \boldsymbol{\omega}_{\mathcal{B}/\mathcal{N}}\right) + \boldsymbol{r}_{Bc/B} \times m_{\mathrm{hub}}\, \ddot{\boldsymbol{r}}_{Bc/B} + \\ + \sum_{i=1}^{M} \left([I_{\mathrm{fuel}_i,\,Fc_i}]\, \dot{\boldsymbol{\omega}}_{\mathcal{B}/\mathcal{N}} + \boldsymbol{\omega}_{\mathcal{B}/\mathcal{N}} \times \left([I_{\mathrm{fuel}_i,\,Fc_i}]\, \boldsymbol{\omega}_{\mathcal{B}/\mathcal{N}}\right) + \boldsymbol{r}_{Fc_i/B} \times m_{\mathrm{fuel}_i}\, \ddot{\boldsymbol{r}}_{Fc_i/B} + \right. \\ \left. + \boldsymbol{r}_{Fc_i/B} \times \dot{m}_{\mathrm{fuel}_i}\, \dot{\boldsymbol{r}}_{Fc_i/B} + [I_{\mathrm{fuel}_i,\,Fc_i}]'\, \boldsymbol{\omega}_{\mathcal{B}/\mathcal{N}}\right) \quad (38)$$

It must be noticed that any relative motion of the particle inside the spacecraft has been neglected and, as a consequence, the effects both of the Coriolis' acceleration and of the whirling motion on the spacecraft dynamics have not been considered. An more detailed dissertation about the impact of these effect can be found in [6].
Additionally, the derivate of the vectors $\boldsymbol{r}_{Bc/B}$ and $\boldsymbol{r}_{Fc_i/B}$ can be computed using the transport theorem between the two reference frames:

$$\dot{\boldsymbol{r}}_{Bc/B} = \boldsymbol{r}'_{Bc/B} + \boldsymbol{\omega}_{\mathcal{B}/\mathcal{N}} \times \boldsymbol{r}_{Bc/B} = \boldsymbol{\omega}_{\mathcal{B}/\mathcal{N}} \times \boldsymbol{r}_{Bc/B} \quad (39)$$

$$\ddot{\boldsymbol{r}}_{Bc/B} = \dot{\boldsymbol{\omega}}_{\mathcal{B}/\mathcal{N}} \times \boldsymbol{r}_{Bc/B} + \boldsymbol{\omega}_{\mathcal{B}/\mathcal{N}} \times \left(\boldsymbol{\omega}_{\mathcal{B}/\mathcal{N}} \times \boldsymbol{r}_{Bc/B}\right) \quad (40)$$

$$\dot{\boldsymbol{r}}_{Fc_i/B} = \boldsymbol{r}'_{Fc_i/B} + \boldsymbol{\omega}_{\mathcal{B}/\mathcal{N}} \times \boldsymbol{r}_{Fc_i/B} \quad (41)$$

$$\ddot{\boldsymbol{r}}_{Fc_i/B} = \boldsymbol{r}''_{Fc_i/B} + 2\,\boldsymbol{\omega}_{\mathcal{B}/\mathcal{N}} \times \boldsymbol{r}'_{Fc_i/B} + \dot{\boldsymbol{\omega}}_{\mathcal{B}/\mathcal{N}} \times \boldsymbol{r}_{Fc_i/B} + \\ + \boldsymbol{\omega}_{\mathcal{B}/\mathcal{N}} \times \left(\boldsymbol{\omega}_{\mathcal{B}/\mathcal{N}} \times \boldsymbol{r}_{Fc_i/B}\right) \quad (42)$$

By substituting equations 40, 41 and 42 in equation 38 can be rewritten:

$$\begin{aligned}\dot{\boldsymbol{H}}_{\mathrm{sc},\,B} = {} & [I_{\mathrm{hub},\,Bc}]\,\dot{\boldsymbol{\omega}}_{\mathcal{B}/\mathcal{N}} + \boldsymbol{\omega}_{\mathcal{B}/\mathcal{N}} \times \left([I_{\mathrm{hub},\,Bc}]\,\boldsymbol{\omega}_{\mathcal{B}/\mathcal{N}}\right) + \\ & + \boldsymbol{r}_{Bc/B} \times m_{\mathrm{hub}}\,\left(\dot{\boldsymbol{\omega}}_{\mathcal{B}/\mathcal{N}} \times \boldsymbol{r}_{Bc/B} + \boldsymbol{\omega}_{\mathcal{B}/\mathcal{N}} \times \left(\boldsymbol{\omega}_{\mathcal{B}/\mathcal{N}} \times \boldsymbol{r}_{Bc/B}\right)\right) + \\ & + \sum_{i=1}^{M}\Big([I_{\mathrm{fuel}_i,\,Fc_i}]\,\dot{\boldsymbol{\omega}}_{\mathcal{B}/\mathcal{N}} + \boldsymbol{\omega}_{\mathcal{B}/\mathcal{N}} \times \left([I_{\mathrm{fuel}_i,\,Fc_i}]\,\boldsymbol{\omega}_{\mathcal{B}/\mathcal{N}}\right) + \\ & + \boldsymbol{r}_{Fc_i/B} \times m_{\mathrm{fuel}_i}\left(\boldsymbol{r}''_{Fc_i/B} + 2\,\boldsymbol{\omega}_{\mathcal{B}/\mathcal{N}} \times \boldsymbol{r}'_{Fc_i/B} + \right. \\ & \left. + \dot{\boldsymbol{\omega}}_{\mathcal{B}/\mathcal{N}} \times \boldsymbol{r}_{Fc_i/B} + \boldsymbol{\omega}_{\mathcal{B}/\mathcal{N}} \times \left(\boldsymbol{\omega}_{\mathcal{B}/\mathcal{N}} \times \boldsymbol{r}_{Fc_i/B}\right)\right) + \\ & + \boldsymbol{r}_{Fc_i/B} \times \dot{m}_{\mathrm{fuel}_i}\left(\boldsymbol{r}'_{Fc_i/B} + \boldsymbol{\omega}_{\mathcal{B}/\mathcal{N}} \times \boldsymbol{r}_{Fc_i/B}\right) + \left[I_{\mathrm{fuel},_i,\,Fc_i}\right]'\boldsymbol{\omega}_{\mathcal{B}/\mathcal{N}}\Big) \end{aligned} \tag{43}$$

In order to compact the equation 43 the following inertia matrices must be defined using the tilde operator to replace the cross product:

$$[I_{\mathrm{hub},\,B}] = [I_{\mathrm{hub},\,Bc}] + m_{\mathrm{hub}}\,\left[\tilde{\boldsymbol{r}}_{Bc/B}\right]\left[\tilde{\boldsymbol{r}}_{Bc/B}\right]^T \tag{44}$$

$$[I_{\mathrm{fuel}_i,\,B}] = [I_{\mathrm{fuel}_i,\,Fc_i}] + m_{\mathrm{fuel}_i}\,\left[\tilde{\boldsymbol{r}}_{Fc_i/B}\right]\left[\tilde{\boldsymbol{r}}_{Fc_i/B}\right]^T \tag{45}$$

$$[I_{\mathrm{sc},\,B}] = [I_{\mathrm{hub},\,B}] + \sum_{i=1}^{M}[I_{\mathrm{fuel}_i,\,B}] \tag{46}$$

Moreover, using the Jacobi identity for the cross product $\mathbf{a} \times (\mathbf{b} \times \mathbf{c}) + \mathbf{b} \times (\mathbf{c} \times \mathbf{a}) + \mathbf{c} \times (\mathbf{a} \times \mathbf{b}) = \mathbf{0}$ the derivative of the fuel inertia in the $\mathcal{B}$ reference frame can be introduced:

$$\begin{aligned}\boldsymbol{r}_{Fc_i/B} \times \left(2\,\boldsymbol{\omega}_{\mathcal{B}/\mathcal{N}} \times \boldsymbol{r}'_{Fc_i/B}\right) = {} & -\boldsymbol{r}_{Fc_i/B} \times \left(\boldsymbol{r}'_{Fc_i/B} \times \boldsymbol{\omega}_{\mathcal{B}/\mathcal{N}}\right) + \\ & + \boldsymbol{r}_{Fc_i/B} \times \left(\boldsymbol{\omega}_{\mathcal{B}/\mathcal{N}} \times \boldsymbol{r}'_{Fc_i/B}\right) = -\boldsymbol{r}_{Fc_i/B} \times \left(\boldsymbol{r}'_{Fc_i/B} \times \boldsymbol{\omega}_{\mathcal{B}/\mathcal{N}}\right) + \\ & - \boldsymbol{r}'_{Fc_i/B} \times \left(\boldsymbol{r}_{Fc_i/B} \times \boldsymbol{\omega}_{\mathcal{B}/\mathcal{N}}\right) + \boldsymbol{\omega}_{\mathcal{B}/\mathcal{N}} \times \left(\boldsymbol{r}_{Fc_i/B} \times \boldsymbol{r}'_{Fc_i/B}\right) \end{aligned} \tag{47}$$

$$\begin{aligned}[I_{\mathrm{fuel}_i,\,B}]' = {} & [I_{\mathrm{fuel}_i,\,Fc_i}] + \dot{m}_{\mathrm{fuel}_i}\,\left[\tilde{\boldsymbol{r}}_{Fc_i/B}\right]\left[\tilde{\boldsymbol{r}}_{Fc_i/B}\right]^T + \\ & + m_{\mathrm{fuel}_i}\left(\left[\tilde{\boldsymbol{r}}_{Fc_i/B}\right]\left[\tilde{\boldsymbol{r}}'_{Fc_i/B}\right]^T + \left[\tilde{\boldsymbol{r}}'_{Fc_i/B}\right]\left[\tilde{\boldsymbol{r}}_{Fc_i/B}\right]^T\right) \end{aligned} \tag{48}$$

Thus, by substituting equations 44, 45, 46, 47 and 48 and developing the expressions:

$$\begin{aligned}\dot{\boldsymbol{H}}_{\mathrm{sc},\,B} = {} & [I_{\mathrm{sc},\,B}]\,\dot{\boldsymbol{\omega}}_{\mathcal{B}/\mathcal{N}} + \left[\tilde{\boldsymbol{\omega}}_{\mathcal{B}/\mathcal{N}}\right][I_{\mathrm{sc},\,B}]\,\boldsymbol{\omega}_{\mathcal{B}/\mathcal{N}} + \sum_{i=1}^{M}\Big(m_{\mathrm{fuel}_i}\,\left[\tilde{\boldsymbol{r}}_{Fc_i/B}\right]\boldsymbol{r}''_{Fc_i/B} + \\ & + \dot{m}_{\mathrm{fuel}_i}\left[\tilde{\boldsymbol{r}}_{Fc_i/B}\right]\boldsymbol{r}'_{Fc_i/B} + [I_{\mathrm{fuel}_i,\,B}]'\,\boldsymbol{\omega}_{\mathcal{B}/\mathcal{N}} + \left[\tilde{\boldsymbol{\omega}}_{\mathcal{B}/\mathcal{N}}\right]\left[\tilde{\boldsymbol{r}}_{Fc_i/B}\right]\boldsymbol{r}'_{Fc_i/B}\Big) \end{aligned} \tag{49}$$

Considering that, at the nozzles's exit, $\dot{\boldsymbol{r}}_{M/B} = \boldsymbol{v}_{exh_j} + \boldsymbol{\omega}_{\mathcal{B}/\mathcal{N}} \times \boldsymbol{r}_{M/B}$ and $\mathrm{d}\dot{m} = -\rho\, \boldsymbol{r}'_{M/B} \cdot \hat{\boldsymbol{n}}\, \mathrm{d}A$, the surface integral can be expressed in term of the nozzles' surface:

$$\int_{A_{\mathrm{exh}}} \rho\, \boldsymbol{r}'_{M/B} \cdot \boldsymbol{n} \left(\boldsymbol{r}_{M/B} \times \dot{\boldsymbol{r}}_{M/B} \right) \mathrm{d}A = -\sum_{j=1}^{N} \int_{\dot{m}_{\mathrm{noz}_j}} \boldsymbol{r}_{M/B} \times \boldsymbol{v}_{\mathrm{exh}_j}\, \mathrm{d}\dot{m} + \\ + \sum_{j=1}^{N} \int_{\dot{m}_{\mathrm{noz}_j}} \boldsymbol{r}_{M/B} \times \left(\boldsymbol{r}_{M/B} \times \boldsymbol{\omega}_{\mathcal{B}/\mathcal{N}} \right) \mathrm{d}\dot{m} \quad (50)$$

Finally the equation of motion 36 can be updated with equations 49 and 50:

$$\dot{\boldsymbol{H}}_{\mathrm{sc},\, B} = \left[I_{\mathrm{sc},\, B} \right] \dot{\boldsymbol{\omega}}_{\mathcal{B}/\mathcal{N}} + \left[\tilde{\boldsymbol{\omega}}_{\mathcal{B}/\mathcal{N}} \right] \left[I_{\mathrm{sc},\, B} \right] \boldsymbol{\omega}_{\mathcal{B}/\mathcal{N}} + \sum_{i=1}^{M} \Big(m_{\mathrm{fuel}_i} \left[\tilde{\boldsymbol{r}}_{Fc_i/B} \right] \boldsymbol{r}''_{Fc_i/B} + \\ + \dot{m}_{\mathrm{fuel}_i} \left[\tilde{\boldsymbol{r}}_{Fc_i/B} \right] \boldsymbol{r}'_{Fc_i/B} + \left[I_{\mathrm{fuel}_i,\, B} \right]' \boldsymbol{\omega}_{\mathcal{B}/\mathcal{N}} + m_{\mathrm{fuel}_i} \left[\tilde{\boldsymbol{\omega}}_{\mathcal{B}/\mathcal{N}} \right] \left[\tilde{\boldsymbol{r}}_{Fc_i/B} \right] \boldsymbol{r}'_{Fc_i/B} \Big) + \\ + \sum_{j=1}^{N} \int_{\dot{m}_{\mathrm{noz}_j}} \left[\tilde{\boldsymbol{r}}_{M/B} \right]^T \boldsymbol{v}_{\mathrm{exh}_j}\, \mathrm{d}\dot{m} + \sum_{j=1}^{N} \int_{\dot{m}_{\mathrm{noz}_j}} \left[\tilde{\boldsymbol{r}}_{M/B} \right] \left[\tilde{\boldsymbol{r}}_{M/B} \right] \boldsymbol{\omega}_{\mathcal{B}/\mathcal{N}}\, \mathrm{d}\dot{m} + \\ + \left[\tilde{\boldsymbol{c}} \right] m_{\mathrm{sc}}\, \ddot{\boldsymbol{r}}_{B/N} = \boldsymbol{L}_{B,\,\mathrm{vol}} + \boldsymbol{L}_{B,\,\mathrm{surf}} \quad (51)$$

The torque of each nozzle can be computed as a part given by the exhausting flow pressure distribution and a second one provided by the lever arm distance from the point B and the application point of the force:

$$\boldsymbol{L}_{B_{\mathrm{thr}_j}} = \boldsymbol{L}_{B_{\mathrm{sc},\ \mathrm{noz}_j}} + \int_{\dot{m}_{\mathrm{noz}_j}} \boldsymbol{r}_{M/B} \times \boldsymbol{v}_{\mathrm{noz}_j}\, \mathrm{d}\dot{m} \quad (52)$$

Furthermore, a term taking into account the angular momentum variation caused by mass depletion can be defined:

$$[K] = \sum_{i=1}^{M} \left[I_{\mathrm{fuel}_i,\, B} \right]' + \sum_{j=1}^{N} \int_{\dot{m}_{\mathrm{noz}_j}} \left[\tilde{\boldsymbol{r}}_{M/B} \right] \left[\tilde{\boldsymbol{r}}_{M/B} \right] \mathrm{d}\dot{m} \quad (53)$$

The second integral in equation 53 can be computed evaluating the momentum exchanged due to the fuel thin disc going out from the nozzle area, coincident in this case with part of the interface surface between the spacecraft and the exhausted fuel:

$$\int_{\dot{m}_{\mathrm{noz}_j}} \left[\tilde{\boldsymbol{r}}_{M/B}\right]\left[\tilde{\boldsymbol{r}}_{M/B}\right]\,\mathrm{d}\dot{m} =$$

$$= \int_{\dot{m}_{\mathrm{noz}_j}} \left(\left[\tilde{\boldsymbol{r}}_{N_j/B}\right] + \left[\tilde{\boldsymbol{r}}_{M/N_j}\right]\right)\left(\left[\tilde{\boldsymbol{r}}_{N_j/B}\right] + \left[\tilde{\boldsymbol{r}}_{M/N_j}\right]\right)\,\mathrm{d}\dot{m} =$$

$$= -\dot{m}_{\mathrm{noz}_j}\left(\left[\tilde{\boldsymbol{r}}_{N_j/B}\right]\left[\tilde{\boldsymbol{r}}_{N_j/B}\right]^T + \frac{A_{\mathrm{noz}_j}}{4\,\pi}\left[BM_j\right]\begin{bmatrix}2&0&0\\0&1&0\\0&0&1\end{bmatrix}\left[BM_j\right]^T\right) \quad (54)$$

where A_{noz_j} is the exiting area of the j-th nozzle and $[BM_j]$ is the change coordinate matrix from the j-th nozzle frame $\mathcal{M}_j$, defined to have its origin in the N_j point and its first axis in the exhausting velocity direction $\boldsymbol{v}_{\mathrm{exh}_j}$, to the $\mathcal{B}$ frame.
Finally the rotational equation of motion can be written:

$$\left[I_{\mathrm{sc},\,B}\right]\dot{\boldsymbol{\omega}}_{\mathcal{B}/\mathcal{N}} + m_{\mathrm{sc}} + \left[\tilde{\boldsymbol{c}}\right]\ddot{\boldsymbol{r}}_{B/N} = \left[\tilde{\boldsymbol{\omega}}_{\mathcal{B}/\mathcal{N}}\right]^T\left[I_{\mathrm{sc},\,B}\right]\boldsymbol{\omega}_{\mathcal{B}/\mathcal{N}} - \left[K\right]\boldsymbol{\omega}_{\mathcal{B}/\mathcal{N}} +$$
$$+ \sum_{i=1}^{M}\Big(m_{\mathrm{fuel}_i}\left[\tilde{\boldsymbol{r}}_{Fc_i/B}\right]^T\boldsymbol{r}''_{Fc_i/B} + m_{\mathrm{fuel}_i}\left[\tilde{\boldsymbol{\omega}}_{\mathcal{B}/\mathcal{N}}\right]^T\left[\tilde{\boldsymbol{r}}_{Fc_i/B}\right]\boldsymbol{r}'_{Fc_i/B} +$$
$$+ \dot{m}_{\mathrm{fuel}_i}\left[\tilde{\boldsymbol{r}}_{Fc_i/B}\right]^T\boldsymbol{r}'_{Fc_i/B}\Big) + \boldsymbol{L}_{B,\,\mathrm{vol}} + \boldsymbol{L}_{B,\,\mathrm{surf}} + \sum_{j=1}^{N}\boldsymbol{L}_{B_{\mathrm{thr}_j}} \quad (55)$$

4.2.1 The $[K]$ term

In this paragraph a brief dissertation about the $[K]$ matrix defined in equation 53 will be developed.
This matrix summarizes the angular momentum variation induced by the mass depletion. It is a symmetric matrix as it is sum of matrices of this type and, as shown in equation 53, it depends directly from the nozzles' position and geometry and from the tanks' mass variation and shape.
In figure 3 a simple but instructive case is shown and it could be useful to clarify the influence of the $[K]$ term and can be analyzed in details in [7] where various tank configurations are considered and a dissertation of the spin and transversal rate is developed to understand the influence of the mass depletion on the system. In all the three cases a cylindrical tank is rotating about its symmetry axis $\hat{\boldsymbol{e}}_3$ with constant angular velocity $\boldsymbol{\omega}_{\mathcal{B}/\mathcal{N}} = \begin{bmatrix}0 & 0 & \omega_{\mathcal{B}/\mathcal{N}_z}\end{bmatrix}^T$ and, at a given time, it starts loosing mass according to the force to be applied. On one hand, the angular momentum transported by a particle at the tank's wall will be:

$$\boldsymbol{H}_{\mathrm{part},\,\mathrm{tank}} = m_{\mathrm{part}}\,\boldsymbol{R}_{\mathrm{tank}} \times \left(\boldsymbol{R}_{\mathrm{tank}} \times \boldsymbol{\omega}_{\mathcal{B}/\mathcal{N}}\right) = m_{\mathrm{part}}\begin{bmatrix}0\\0\\R^2_{\mathrm{tank}}\,\omega_{\mathcal{B}/\mathcal{N}_z}\end{bmatrix} \quad (56)$$

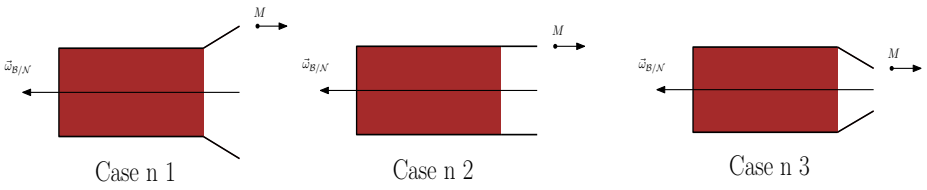

Figure 3: Cases of the influence of the $[K]$ matrix on the system dynamics.

where m_{part} is the particle mass and $\boldsymbol{R}_{\text{tank}}$ is the cylinder radius.
On the other, the angular momentum of the same particle at the nozzle's exit could be easily written as follows:

$$\boldsymbol{H}_{\text{part, noz}} = m_{\text{part}}\, \boldsymbol{R}_{\text{noz}} \times \left(\boldsymbol{R}_{\text{noz}} \times \boldsymbol{\omega}_{\mathcal{B}/\mathcal{N}} + \boldsymbol{v}_{\text{exh}}\right) = m_{\text{part}} \begin{bmatrix} 0 \\ 0 \\ R_{\text{noz}}^2\, \omega_{\mathcal{B}/\mathcal{N}_z} \end{bmatrix} \tag{57}$$

where $\boldsymbol{R}_{\text{noz}}$ is the nozzle radius.
Obviously the angular momentum variation is equal to the amount of it transported throughout the surface control by the particles. Intuitively, three different cases can be distinguished:

1. If $R_{\text{tank}} < R_{\text{noz}}$, the particle is transporting more angular momentum than the one owned previously inside the tank from the same particle as the distance from the symmetry axis $\hat{\boldsymbol{e}}_3$ is bigger. As a consequence, the body tends to spin down and asymptotically stabilize the motion.

2. If $R_{\text{tank}} = R_{\text{noz}}$, the same amount of angular momentum possessed inside the tank by the particle is ejected from the nozzle and, consequently, the body does not modify its state of motion.

3. If $R_{\text{tank}} > R_{\text{noz}}$, the angular momentum difference is smaller than zero and the system spins up to compensate this gap.

5 Fuel supply architecture and implementation

From a program implementation prospective the tank mass flow and their derivatives must be computed once a maneuver is performed to evaluate the different terms in the equations of motion. By using this approach the $j-$th nozzle mass flow will be considered a known quantity and could be computed from the thrust and the nozzle's properties, i.e. I_{sp_j} and $\boldsymbol{v}_{\text{noz}_j}$.
If a matrix notation is used:

$$\dot{\boldsymbol{m}}_{\text{fuel}} = [A]\ \dot{\boldsymbol{m}}_{\text{noz}} \tag{58}$$

where $[A]$ is a matrix linking the tanks' mass flows and nozzles' ones.
A fundamental property of the matrix A can be established from the definition

of $\dot{m}_{\text{fuel}}$:

$$\sum_{i=1}^{M} \dot{m}_{\text{fuel}_i} = \sum_{i=1}^{M} \sum_{j=1}^{N} A_{ij} \dot{m}_{\text{noz}_j} = \sum_{j=1}^{N} \dot{m}_{\text{noz}_j} \quad \Rightarrow \quad \sum_{i=0}^{M} A_{ij} = 1 \quad \forall j \in (1, N) \tag{59}$$

The previous relation is a direct consequence of the mass flow conservation between the tanks and the nozzles.
From the previous relation, the first derivative of mass flows can be easily computed:

$$\ddot{\boldsymbol{m}}_{\text{fuel}} = [A]\ \ddot{\boldsymbol{m}}_{\text{noz}} + [\dot{A}]\dot{\boldsymbol{m}}_{\text{noz}} \tag{60}$$

In the following analysis the $[A]$ will be considered constant with time, i.e. $[\dot{A}] = 0$. In figure 4 an example of a possible distribution system is shown.

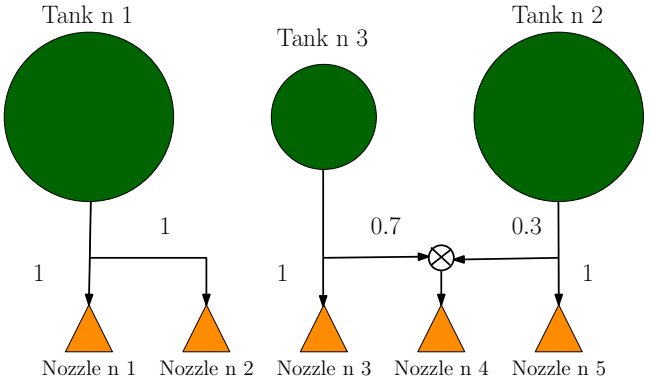

Figure 4: An example of the distribution system among tanks and nozzles with numerical values.

Taking to account this schematic representation and the fact that each component of the matrix $[A]_{ij}$ represent the percentage of fuel ejected by the nozzle j given from the tank i, an example can be easily developed.The system of equation is:

$$\begin{cases} \dot{m}_{\text{fuel}_1} = \dot{m}_{\text{noz}_1} + \dot{m}_{\text{noz}_2} \\ \dot{m}_{\text{fuel}_2} = 0.3\, \dot{m}_{\text{noz}_4} + \dot{m}_{\text{noz}_5} \\ \dot{m}_{\text{fuel}_3} = \dot{m}_{\text{noz}_3} + 0.7\, \dot{m}_{\text{noz}_4} \end{cases} \tag{61}$$

Thus, the $[A]$ matrix is:

$$[A] = \begin{bmatrix} 1 & 1 & 0 & 0 & 0 \\ 0 & 0 & 0 & 0.3 & 1 \\ 0 & 0 & 1 & 0.7 & 0 \end{bmatrix} \tag{62}$$

6 Control feedback law

Once equations have been gathered, control can be included to reach the desired reference state despite the disturbances applied on the spacecraft.
According to reference [8], a Modified Rodrigues Parameters (MRP) feedback control law has been chosen as it can always assure global asymptotic stability avoiding singularities. If a reference frame $\mathcal{R}$ is defined, the control can be expressed as follows:

$$\boldsymbol{u} = -K\,\boldsymbol{\sigma}_{\mathcal{B}/\mathcal{R}} - P\,\boldsymbol{\omega}_{\mathcal{B}/\mathcal{R}} \tag{63}$$

where $\boldsymbol{\sigma}_{\mathcal{B}/\mathcal{R}}$ is the MRP defining the attitude from the $\mathcal{R}$ frame to the $\mathcal{B}$ one and $\boldsymbol{\omega}_{\mathcal{B}/\mathcal{R}}$ is the angular velocity of the $\mathcal{B}$ frame about the $\mathcal{R}$ one. The importance of using a $\mathcal{R}$ frame instead the inertial one $\mathcal{N}$ lies in the possibility of moving the reference frame $\mathcal{R}$ about the latter to let the spacecraft orient its axis as desired in the euclidean space imposing both the attitude and the angular velocity. A clear example of this concept could be a reference frame $\mathcal{R}$ spinning about the inertial frame $\mathcal{N}$.
In order to evaluate the control torque the attitude $\boldsymbol{\sigma}_{\mathcal{B}/\mathcal{R}}$ and the angular velocity $\boldsymbol{\omega}_{\mathcal{B}/\mathcal{R}}$ must be computed. By considering known $\boldsymbol{\sigma}_{\mathcal{R}/\mathcal{N}}$ and $\boldsymbol{\omega}_{\mathcal{R}/\mathcal{N}}$, the needed variables can be calculated as follows [8, 9]:

$$\begin{aligned}\boldsymbol{\sigma}_{\mathcal{B}/\mathcal{R}} &= \boldsymbol{\sigma}_{\mathcal{B}/\mathcal{N}} \odot \boldsymbol{\sigma}_{\mathcal{R}/\mathcal{N}} = \\ &= \frac{\left(1 - \boldsymbol{\sigma}_{\mathcal{B}/\mathcal{N}}^T \boldsymbol{\sigma}_{\mathcal{B}/\mathcal{N}}\right)\boldsymbol{\sigma}_{\mathcal{R}/\mathcal{N}} + \left(1 - \boldsymbol{\sigma}_{\mathcal{R}/\mathcal{N}}^T \boldsymbol{\sigma}_{\mathcal{R}/\mathcal{N}}\right)\boldsymbol{\sigma}_{\mathcal{B}/\mathcal{N}} - 2\,\boldsymbol{\sigma}_{\mathcal{R}/\mathcal{N}} \times \boldsymbol{\sigma}_{\mathcal{B}/\mathcal{N}}}{1 + \left(\boldsymbol{\sigma}_{\mathcal{B}/\mathcal{N}}^T \boldsymbol{\sigma}_{\mathcal{B}/\mathcal{N}}\right)\left(\boldsymbol{\sigma}_{\mathcal{R}/\mathcal{N}}^T \boldsymbol{\sigma}_{\mathcal{R}/\mathcal{N}}\right) + 2\,\boldsymbol{\sigma}_{\mathcal{B}/\mathcal{N}}^T \boldsymbol{\sigma}_{\mathcal{R}/\mathcal{N}}}\end{aligned} \tag{64}$$

$$\boldsymbol{\omega}_{\mathcal{B}/\mathcal{R}} = \boldsymbol{\omega}_{\mathcal{B}/\mathcal{N}} - \boldsymbol{\omega}_{\mathcal{R}/\mathcal{N}} \tag{65}$$

where, in case of singular representation of the MRP set $\boldsymbol{\sigma}_{\mathcal{B}/\mathcal{R}}$, one of the two initial MRP can be switched to the shadow representation ${}^S\boldsymbol{\sigma}_{\mathcal{B}/\mathcal{N}}$ defined by:

$${}^S\boldsymbol{\sigma} = -\frac{\boldsymbol{\sigma}}{\boldsymbol{\sigma}^T\,\boldsymbol{\sigma}} \tag{66}$$

For a detailed dissertation and the kinematic relations among the different angular representations, the references [8] could be used.
The control torque might be concretely provided to the spacecraft through various devices and, in the present work, a thruster-based control will be implemented to underline the main features of mass depletion.
The challenge of this approach is to find out the needed forces from a given torque. The following algorithm has been provided by Dr. Hanspeter Schaub and has not be developed by the author.
By assuming a series of P ACS thrusters, the position of the k-th nozzle can be labeled $\boldsymbol{r}_{N_k/B}$ and the k-th force is given by:

$$\boldsymbol{F}_{\text{thr}_k} = F_{\text{thr}_k}\,\hat{\boldsymbol{g}}_k = F_{\text{thr}_k}\,[BM_k]\,\hat{\boldsymbol{m}}_{1_k} \tag{67}$$

where $\hat{\boldsymbol{m}}_{1_k}$ is the first versor of the k-th ADC (Attitude Control System) thruster's reference frame $\mathcal{M}_k$. Consequently, the torque generated can be easily computed:

$$\boldsymbol{L}_{B_{\text{thr}_k}} = \boldsymbol{r}_{N_k/B} \times F_{\text{thr}_k} \hat{\boldsymbol{g}}_k \tag{68}$$

If a set of ortho-normal, i.e. $\hat{\boldsymbol{c}}_h \cdot \hat{\boldsymbol{c}}_h = 1$ and $\hat{\boldsymbol{c}}_h \cdot \hat{\boldsymbol{c}}_r =$ if $h \neq r$ for $r\,, h \in (1, 3)$, axis is chosen the total torque provided by the thrusters about the $\hat{\boldsymbol{c}}_h$ is:

$$\boldsymbol{L}_{B_{\text{thr}}} \cdot \hat{\boldsymbol{c}}_h = \sum_{k=1}^{P} \boldsymbol{L}_{B_{\text{thr}_k}} \cdot \hat{\boldsymbol{c}}_h = \sum_{k=1}^{P} \left(\boldsymbol{r}_{N_k/B} \times \hat{\boldsymbol{g}}_k\right) \cdot \hat{\boldsymbol{c}}_h F_{\text{thr}_k} = \sum_{k=1}^{P} d_k F_{\text{thr}_k} \tag{69}$$

In a matrix form:

$$\boldsymbol{L}_{B_{\text{thr}}} \cdot \hat{\boldsymbol{c}}_h = [D]\, \boldsymbol{F}_{\text{thr}} \tag{70}$$

The first step to compute the forces is to find which thrusters could provide positive F_{thr_k}, thus in accord with the definition of F_{thr_k} as magnitude of the force vector. This can be actually achieved by a minimum norm solution to produce the needed control torque:

$$\boldsymbol{F}_{\text{thr}} = [D]^T \left([D]\,[D]^T\right)^{-1} \boldsymbol{u} \cdot \hat{\boldsymbol{c}}_h \tag{71}$$

By considering the $\overline{P}$ thrusters providing positive magnitude from Equation 71 and calling $\overline{\boldsymbol{F}}_{\text{thr}}$ the vector containing their magnitude, $\left[\,\overline{D}\,\right]$ is a $3 \times \overline{P}$ matrix defined as follows:

$$\overline{\boldsymbol{d}}_k = \boldsymbol{r}_{N_k/B} \times \hat{\boldsymbol{g}}_k \tag{72}$$

From this definition, the thruster mapping is:

$$\left[\,\overline{D}\,\right] \overline{\boldsymbol{F}}_{\text{thr}} = \hat{\boldsymbol{c}}_h \left(\boldsymbol{u} \cdot \hat{\boldsymbol{c}}_h\right) \tag{73}$$

At the same time, the thruster should not produce a net force on the spacecraft in order not to influence the translational motion. Thus:

$$\overline{\boldsymbol{F}} = \left[\,\overline{G}\,\right] \overline{\boldsymbol{F}}_{\text{thr}} = 0 \tag{74}$$

where $\left[\overline{G}\right]$ is a $3 \times \overline{P}$ matrix containing the thrust's direction.
In order to minimize the net force applied on the spacecraft with the constrain of obtaining a given torque, the following functional must be minimized:

$$J = \frac{1}{2} \overline{\boldsymbol{F}}_{\text{thr}}^T \left[\,\overline{G}\,\right]^T \left[\,\overline{G}\,\right] \overline{\boldsymbol{F}}_{\text{thr}} + \boldsymbol{\lambda}^T \left(\left[\,\overline{D}\,\right] \overline{\boldsymbol{F}}_{thr} - \hat{\boldsymbol{c}}_h \left(\boldsymbol{u} \cdot \hat{\boldsymbol{c}}_h\right)\right) \tag{75}$$

where λ is the 3×1 Lagrange multiplier vector. By imposing its gradient equals to zero, the set of forces provided by the chosen nozzles can be computed.

$$\begin{bmatrix} \overline{G}^T \overline{G} & \overline{D}^T \\ \overline{D} & \boldsymbol{0}_{3\times 3} \end{bmatrix} \begin{bmatrix} \boldsymbol{F}_{\text{thr}} \\ \boldsymbol{\lambda} \end{bmatrix} = \begin{bmatrix} \boldsymbol{0}_{\overline{P}\times 1} \\ \hat{\boldsymbol{c}}_h \left(\boldsymbol{u} \cdot \hat{\boldsymbol{c}}_h\right) \end{bmatrix} \tag{76}$$

This procedure is applied to every component of the control $\boldsymbol{u}$ and, finally, the net force generated can be computed summing the force generated from the P nozzle:

$$\boldsymbol{F}_{\text{net}} = \sum_{k=1}^{P} \boldsymbol{F}_{\text{thr}_k} \tag{77}$$

It must be noticed that this approach does not require a symmetric ADC thrusters' configuration and can be applied to whichever set of thruster minimizing the net force and providing the needed control torque.

7 Tank models

Different tank models could be developed to perfectly suit the needs of the spacecraft's fuel chain configuration. In the present paper five reservoir models will be considered as examples and their properties, such as inertia variation and barycenter motion, will be gathered.
The models and their main hypothesis are presented below:

- The constant tank's volume model where a spherical reservoir maintains a fixed geometry, i.e. a constant radius, and a fixed barycenter.
- The constant fuel's density model where a spherical tank keeps its geometrical shape but gradually change its volume, so its radius, to maintain constant the density of the fuel and it has a fixed center of mass.
- The emptying tank model where the fuel leaks out from an outlet in the spherical reservoir and the quantity of fuel decrease perpendicularly to the output direction modifying the barycenter position and the body's inertia accordingly to the mass distribution inside the tank.
- The uniform burn cylinder model where a cylindrical tank does not change its geometrical shape and volume but the gas gradually decrease its density. As a consequence, the fuel barycenter remains fixed and the inertia varies accordingly to the mass variation.
- The centrifugal burn cylinder model where a cylindrical tank is considered and the fuel burns radially from the center until the walls without breaking the tank's symmetry. The inertia tensor derivative is computed from these hypothesis and the barycenter remains in its initial position because the symmetry is conserved.

7.1 The constant tank's volume model

This model takes into account the variation of the fuel inside considering no variation of the volume off the tank. By looking at Figure 5:

$$V_{\text{tank}} = cost \quad \Rightarrow \quad R_{\text{tank}} = cost \tag{78}$$

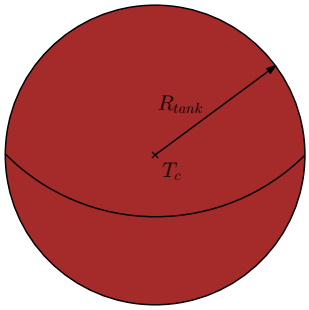

Figure 5: Geometrical properties of the constant density sphere.

$$[I_{\text{fuel, }Tc}] = \frac{2}{5}\, m_{\text{fuel}}\, R^2_{\text{tank}}\, [\mathbb{1}_{3\times 3}] \tag{79}$$

$$[I_{\text{fuel, }Tc}]' = \frac{2}{5}\, \dot{m}_{\text{fuel}}\, R^2_{\text{tank}}\, [\mathbb{1}_{3\times 3}] \tag{80}$$

Moreover the position of the center of mass of the tank does not change, so:

$$\boldsymbol{r}'_{Tc/B} = 0 \qquad\qquad \boldsymbol{r}''_{Tc/B} = 0 \tag{81}$$

7.2 The constant fuel's density model

The second model considers a shape-changing tank adapting itself to keep the fuel's density constant. Thus,according to Figure 6:

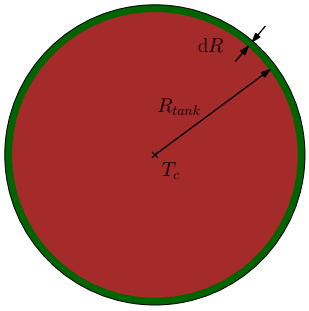

Figure 6: Geometrical properties of the constant density sphere.

$$\begin{cases} \dot{V}_{\text{tank}} = \frac{\dot{m}_{\text{fuel}}}{\rho_{\text{fuel}}} \\ \dot{V}_{\text{tank}} = 4\,\pi\, R^2_{\text{tank}}\, \dot{R}_{\text{tank}} \end{cases} \qquad \Rightarrow \qquad \dot{R}_{\text{tank}} = \frac{\dot{m}_{\text{fuel}}}{4\pi\, R^2_{\text{tank}}\, \rho_{\text{fuel}}} \tag{82}$$

As a consequence:

$$[I_{\text{fuel, }Tc}] = \frac{2}{5}\, m_{\text{fuel}}\, R^2_{\text{tank}}\, [\mathbb{1}_{3\times 3}] \tag{83}$$

$$[I_{\text{fuel},\,Tc}]' = \frac{2}{5}\left(R_{\text{tank}}^2 + \frac{m_{\text{fuel}}}{2\pi\, R_{\text{tank}}\,\rho_{\text{fuel}}}\right)\dot{m}_{\text{fuel}}\,[\mathbb{1}_{3\times3}] =$$
$$= \frac{2}{5}\left(R_{\text{tank}}^2 + \frac{2}{3}\,R_{\text{tank}}^2\right)\dot{m}_{\text{fuel}}\,[\mathbb{1}_{3\times3}] = \frac{2}{3}\dot{m}_{\text{fuel}}R_{\text{tank}}^2\,[\mathbb{1}_{3\times3}] \quad (84)$$

As in the previous model:

$$\boldsymbol{r}'_{Tc/B} = 0 \qquad\qquad \boldsymbol{r}''_{Tc/B} = 0 \quad (85)$$

7.3 The emptying tank model

In this case the mass variation stats from the opposite point to the outlet, that will be called from now on the pole, perpendicularly to the vector connecting the pole and the outlet.
The following notation will be used: $\theta \in (0\,,\pi)$ will be the latitude angle counted from the pole till the outlet, $\phi \in (0\,,2\,\pi)$ will note the longitude angle, the radius will be $r \in (0,\, R_{\text{tank}})$. Moreover the θ^* will denote the angle between the pole and the circumference of the fuel's free surface. The volume $\mathcal{V}$ and the center of mass of the tank can be computed using notations in figure 7:

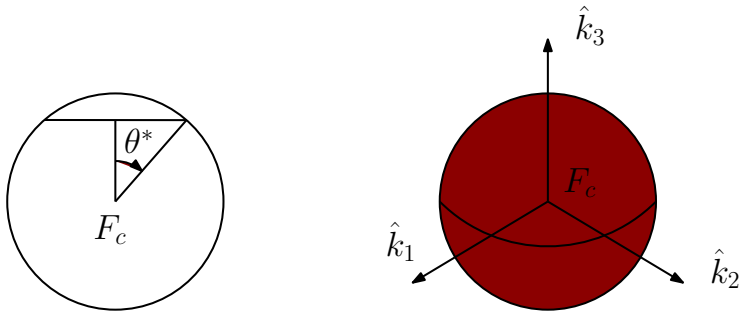

Figure 7: Geometrical properties of the emptying tank model.

$$\mathcal{V}(\theta^*) = \int_0^{2\,\pi}\int_0^{\theta^*}\int_0^{R_{\text{tank}}\frac{\cos\theta^*}{\cos\theta}} r^2\,\sin\theta\,\mathrm{d}\theta\,\mathrm{d}\phi\,\mathrm{d}r +$$
$$+\int_0^{2\,\pi}\int_{\theta^*}^{\pi}\int_0^{R_{\text{tank}}} r^2\,\sin\theta\,\mathrm{d}\theta\,\mathrm{d}\phi\,\mathrm{d}r = \frac{2\,\pi\,R_{\text{tank}}^3}{3}\left[1 + \frac{3}{2}\cos\theta^* - \frac{1}{2}\cos^3\theta^*\right] \quad (86)$$

$$\boldsymbol{r}_{Tc/B}\cdot\hat{\boldsymbol{k}}_3 = \boldsymbol{r}_{Tc'/B}\cdot\hat{\boldsymbol{k}}_3 + \frac{1}{\mathcal{V}(\theta^*)}\left(\int_0^{2\,\pi}\int_0^{\theta^*}\int_0^{R_{\rm tank}\frac{\cos\theta^*}{\cos\theta}} r^3\,\sin\theta\cos\theta\,\mathrm{d}\theta\,\mathrm{d}\phi\,\mathrm{d}r + \right.$$
$$\left. + \int_0^{2\,\pi}\int_{\theta^*}^{\pi}\int_0^{R_{\rm tank}} r^3\,\sin\theta\cos\theta\,\mathrm{d}\theta\,\mathrm{d}\phi\,\mathrm{d}r\right) = \frac{\pi\,R_{\rm tank}^4}{4\,\mathcal{V}(\theta^*)}\left[2\,\cos^2\theta^* - \cos^4\theta^* - 1\right] \tag{87}$$

where $\hat{\boldsymbol{k}}_3$ is the outlet-to-pole axis of the reference frame of the sphere and $\boldsymbol{r}_{Tc'/B}$ the constant vector from B to the center of the sphere.
Considering that $m_{\rm fuel} = \rho_{\rm fuel}\mathcal{V}$, the derivatives in the $\mathcal{B}$ reference frame can be performed:

$$\boldsymbol{r}'_{Tc/B}\cdot\hat{\boldsymbol{k}}_3 = -\frac{\pi\,R_{\rm tank}^4\,\rho_{\rm fuel}}{4\,m_{\rm fuel}^2}\left[4\,m_{\rm fuel}\dot{\theta^*}\,\sin^3\theta^*\cos\theta^* + \right.$$
$$\left. + \dot{m}_{\rm fuel}\left(2\,\cos^2\theta^* - \cos^4\theta^* - 1\right)\right] \tag{88}$$

$$\boldsymbol{r}''_{Tc/B}\cdot\hat{\boldsymbol{k}}_3 = -\frac{\pi\,R_{\rm tank}^4\,\rho_{\rm fuel}}{2\,m_{\rm fuel}^3}\left[4\,m_{\rm fuel}\sin^3\theta^*\cos\theta^*\left(\ddot{\theta^*}\,m_{\rm fuel} - 2\,\dot{\theta^*}\,\dot{m}_{\rm fuel}\right) + \right.$$
$$-4\,m_{\rm fuel}^2\,\dot{\theta^*}^2\sin^2\theta^*\left(3\,\cos^2\theta^* - \sin^2\theta^*\right) +$$
$$\left. + \left(2\,\cos^2\theta^* - \cos^4\theta^* - 1\right)\left(m_{\rm fuel}\ddot{m}_{\rm fuel} - 2\,\dot{m}_{\rm fuel}^2\right)\right] \tag{89}$$

The relation among $\dot{m}_{\rm fuel}$, $\ddot{m}_{\rm fuel}$, $\dot{\theta^*}$ and $\ddot{\theta^*}$ is deduced from the derivation of the relation between the volume $\mathcal{V}$ and $m_{\rm fuel}$:

$$m_{\rm fuel} = \rho_{\rm fuel}\mathcal{V}(\theta^*) \quad \Rightarrow \quad \dot{m}_{\rm fuel} = \rho_{\rm fuel}\dot{\mathcal{V}}(\theta^*)$$
$$\dot{m}_{\rm fuel} = -\pi\,\rho_{\rm fuel}R_{\rm tank}^3\sin^3\theta^*\,\dot{\theta}^* \tag{90}$$

$$\ddot{m}_{\rm fuel} = -\pi\,\rho_{\rm fuel}R_{\rm tank}^3\sin^2\theta^*\left(\ddot{\theta^*}\sin\theta^* + 3\,\dot{\theta^*}^2\cos\theta^*\right) \tag{91}$$

Finally θ^* can be found:

$$m_{\rm fuel} = \rho_{\rm fuel}\mathcal{V}(\theta^*) \;\Rightarrow\; m_{\rm fuel} = \frac{2}{3}\pi\,\rho_{\rm fuel}\,R_{\rm tank}^3\left[1 + \frac{3}{2}\cos\theta^* - \frac{1}{2}\cos^3\theta^*\right] \tag{92}$$

As far as the inertia concerns:

$$I_{3\,3} = \rho_{\rm fuel}\left(\int_0^{2\,\pi}\int_0^{\theta^*}\int_0^{R_{\rm tank}\frac{\cos\theta^*}{\cos\theta}} r^4\,\sin^3\theta\,\mathrm{d}\theta\,\mathrm{d}\phi\,\mathrm{d}r + \right.$$
$$\left. + \int_0^{2\,\pi}\int_{\theta^*}^{\pi}\int_0^{R_{\rm tank}} r^4\,\sin^3\theta\,\mathrm{d}\theta\,\mathrm{d}\phi\,\mathrm{d}r\right) =$$
$$= \frac{2}{5}\pi\,\rho_{\rm fuel}R_{\rm tank}^5\left[\frac{2}{5} + \frac{1}{4}\cos\theta^*\sin^4\theta^* - \frac{1}{12}\left(\cos 3\theta^* - 9\cos\theta^*\right)\right] \tag{93}$$

$$I_{2\,2} = \rho_{\text{fuel}} \left(\int_0^{2\,\pi} \int_0^{\theta^*} \int_0^{R_{\text{tank}} \frac{\cos\theta^*}{\cos\theta}} r^4 \, \left(\sin\theta - \sin^3\theta \sin^2\phi \right) \, \mathrm{d}\theta \, \mathrm{d}\phi \, \mathrm{d}r + \right.$$
$$\left. + \int_0^{2\,\pi} \int_{\theta^*}^{\pi} \int_0^{R_{\text{tank}}} r^4 \, \left(\sin\theta - \sin^3\theta \sin^2\phi \right) \, \mathrm{d}\theta \, \mathrm{d}\phi \, \mathrm{d}r \right) = \frac{2}{5}\pi \, \rho_{\text{fuel}} R_{\text{tank}}^5 \left[\frac{2}{3} + \right.$$
$$\left. - \frac{1}{4}\cos^5\theta^* + \frac{1}{24}\left(\cos 3\theta^* - 9\cos\theta^*\right) + \frac{5}{4}\cos\theta^* + \frac{1}{8}\cos\theta^* \sin^4\theta^* \right] \quad (94)$$

$$I_{1\,1} = \rho_{\text{fuel}} \left(\int_0^{2\,\pi} \int_0^{\theta^*} \int_0^{R_{\text{tank}} \frac{\cos\theta^*}{\cos\theta}} r^4 \, \left(\sin\theta - \sin^3\theta \cos^2\phi \right) \, \mathrm{d}\theta \, \mathrm{d}\phi \, \mathrm{d}r + \right.$$
$$\left. + \int_0^{2\,\pi} \int_{\theta^*}^{\pi} \int_0^{R_{\text{tank}}} r^4 \, \left(\sin\theta - \sin^3\theta \cos^2\phi \right) \, \mathrm{d}\theta \, \mathrm{d}\phi \, \mathrm{d}r \right) = I_{2\,2} \quad (95)$$

$$I_{1\,2} = \rho_{\text{fuel}} \left(\int_0^{2\,\pi} \int_0^{\theta^*} \int_0^{R_{\text{tank}} \frac{\cos\theta^*}{\cos\theta}} r^4 \, \sin^3\theta \cos\phi \sin\phi \, \mathrm{d}\theta \, \mathrm{d}\phi \, \mathrm{d}r + \right.$$
$$\left. + \int_0^{2\,\pi} \int_{\theta^*}^{\pi} \int_0^{R_{\text{tank}}} r^4 \, \sin^3\theta \cos\phi \sin\phi \, \mathrm{d}\theta \, \mathrm{d}\phi \, \mathrm{d}r \right) = 0 \quad (96)$$

$$I_{1\,3} = \rho_{\text{fuel}} \left(\int_0^{2\,\pi} \int_0^{\theta^*} \int_0^{R_{\text{tank}} \frac{\cos\theta^*}{\cos\theta}} r^4 \, \sin^2\theta \cos\theta \cos\phi \, \mathrm{d}\theta \, \mathrm{d}\phi \, \mathrm{d}r + \right.$$
$$\left. + \int_0^{2\,\pi} \int_{\theta^*}^{\pi} \int_0^{R_{\text{tank}}} r^4 \, \sin^2\theta \cos\theta \cos\phi \, \mathrm{d}\theta \, \mathrm{d}\phi \, \mathrm{d}r \, \right) = 0 \quad (97)$$

$$I_{2\,3} \;=\; \rho_{\text{fuel}} \int_0^{2\,\pi} \int_0^{\theta^*} \int_0^{R_{\text{tank}} \frac{\cos\theta^*}{\cos\theta}} r^4 \, \sin^2\theta \cos\theta \sin\phi \, \mathrm{d}\theta \, \mathrm{d}\phi \, \mathrm{d}r \;=\; 0 \quad (98)$$

because $\int_0^{2\,\pi} \cos\phi \sin\phi = \int_0^{2\,\pi} \sin\phi = \int_0^{2\,\pi} \cos\phi = 0$.
From those calculations the derivatives, in the tank reference frame, can be computed:

$$I'_{3\,3} = \frac{2}{5}\pi \, \rho_{\text{fuel}} R_{\text{tank}}^5 \, \dot{\theta^*} \left[\cos^2\theta^* \sin^3\theta^* - \frac{1}{4}\sin^5\theta^* + \frac{1}{4}\sin 3\theta^* - \frac{3}{4}\sin\theta^* \right] \quad (99)$$

$$I'_{2\,2} = I'_{1\,1} = \frac{2}{5}\pi\,\rho_{\text{fuel}} R^5_{\text{tank}}\,\dot{\theta^*}\left[\frac{5}{4}\sin\theta^*\cos\theta^* - \frac{5}{4}\sin\theta^* - \frac{1}{8}\sin 3\theta^* + \right.$$
$$\left. + \frac{3}{8}\sin\theta^* + \frac{1}{2}\cos^2\theta^*\sin^3\theta^* - \frac{1}{8}\sin^5\theta^*\right] \quad (100)$$

7.4 Uniform burn cylinder

This model consider a cylindrical tank whose geometry remains constant while fuel density changes. From these considerations and by looking at Figure 8, the

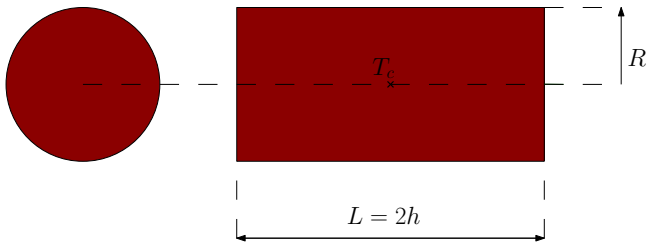

Figure 8: Geometrical properties of the uniform burn cylinder

inertia tensor and its derivative could be evaluated:

$$I_{1\,1} = I_{2\,2} = m_{\text{fuel}}\left[\frac{R^2}{4} + \frac{h^2}{3}\right] \qquad I_{3\,3} = m_{\text{fuel}}\,\frac{R^2}{2} \quad (101)$$

$$I'_{1\,1} = I_{2\,2} = \dot{m}_{\text{fuel}}\left[\frac{R^2}{4} + \frac{h^2}{3}\right] \qquad I'_{3\,3} = \dot{m}_{\text{fuel}}\,\frac{R^2}{2} \quad (102)$$

where R is the cylinder radius and h its half-height.
Moreover, as the position of the center of mass of the tank does not change:

$$\boldsymbol{r}'_{Tc/B} = 0 \qquad \boldsymbol{r}''_{Tc/B} = 0 \quad (103)$$

7.5 Centrifugal burn cylinder

The present model consider a cylinder filled with propellant burning radially from the center to the edge. The geometry properties and their nomenclature can be seen in Figure 9.

By denoting r the distance of the fuel surface from the axis of the cylinder, this quantity can be easily computed from the amount of mass in the tank:

$$r = \sqrt{R^2 - \frac{m_{\text{fuel}}}{2\,\pi\,\rho\,h}} \quad (104)$$

where R is the cylinder radius, h its half-height and ρ the fuel density.
As in the previous models, the time derivative of r can be gathered from volume-mass relation:

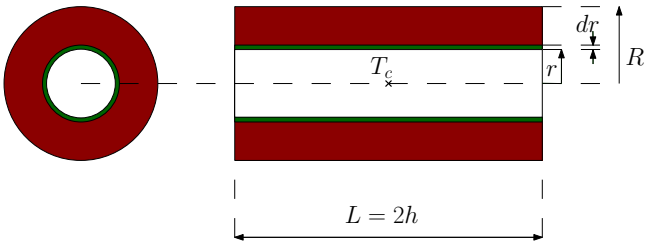

Figure 9: Geometrical properties of the centrifugal burn cylinder

$$\dot{m}_{\text{fuel}} = -4\pi\rho\, h\, r\, \dot{r} \tag{105}$$

As a consequence:

$$I_{1\,1} = I_{2\,2} = m_{\text{fuel}} \left[\frac{R^2 + r^2}{4} + \frac{h^2}{3}\right] \tag{106}$$

$$I_{3\,3} = m_{\text{fuel}} \left[\frac{R^2 + r^2}{2}\right] \tag{107}$$

Moreover, their time derivatives in the tank's reference frame can be computed:

$$I'_{1\,1} = I'_{2\,2} = \dot{m}_{\text{fuel}} \left[\frac{r^2}{2} + \frac{h^2}{3}\right] \tag{108}$$

$$I'_{3\,3} = \dot{m}_{\text{fuel}}\, r^2 \tag{109}$$

Finally, the tank's center of mass does not move as the mass variation is symmetric. Thus:

$$\boldsymbol{r}'_{Tc/B} = 0 \qquad\qquad \boldsymbol{r}''_{Tc/B} = 0 \tag{110}$$

8 Thruster models

The present section presents the thruster's model developed and used in the present work.
Some general properties of the thrusters are here summarized. The thrust will be assumed to follow the specif impulse relation expressed in Equation 27. As a consequence, the impulse, and thus the velocity variation, can be easily computed:

$$\Delta\,\boldsymbol{v} = I_{\text{sp}}\, g_0\, \frac{\boldsymbol{v}_{\text{exh}}}{v_{\text{exh}}} \int_{m_{\text{in}}}^{m_{\text{fin}}} \frac{\mathrm{d}m}{m} = I_{\text{sp}}\, g_0\, \frac{\boldsymbol{v}_{\text{exh}}}{v_{\text{exh}}} \ln\left(\frac{m_{\text{fin}}}{m_{\text{in}}}\right) \tag{111}$$

where m_{in} is the initial mass of the spacecraft and m_{fin} is the final one. The equation is normally projected on the force axis to obtain the well-known scalar equation:

$$\Delta\, v = I_{\text{sp}}\, g_0\, \ln\left(\frac{m_{\text{in}}}{m_{\text{fin}}}\right) \tag{112}$$

It must be underlined that this equation is not dependent from the force law applied on the spacecraft as far as the specific impulse relation stands.
Two simple examples of thruster are presented briefly in the list below and then exposed in the following paragraphs.

- The impulsive thruster model where the thrust is immediately generated during the firing time.
- The ramping thruster model where, once the valve is opened to provide thrust, a time span of response Δt_{resp} is required to acquire the steady state.

Moreover the modularity and adaptability of the code allow the use of complex models which could be implemented directly from the user.

8.1 Impulsive model

This section presents the simplest model developed to perform satellite maneuvers. The thrust has the following expression:

$$\boldsymbol{F}(t) = \begin{cases} I_{\text{sp}}\, g_0\, \dot{m}_{\text{fuel}}\, \frac{\boldsymbol{v}_{\text{exh}}}{v_{\text{exh}}} & \text{if} \quad t_{\text{in}\,\text{fir}} \leq t \leq t_{\text{fin}\,\text{fir}} \\ 0 & \text{otherwise} \end{cases} \tag{113}$$

where $t_{\text{in}\,\text{fir}}$ is the initial firing time and $t_{\text{fin}\,\text{fir}}$ is the final firing time.

The dynamic characteristics associated with this type of thruster are presented in Figures 10. The absence of $\ddot{m}_{\text{fuel}}$ is a simplification of the singular derivative that could be obtained from the step function. This lead to a rapid and easier implementation without loosing precious details during the simulation.

8.2 Ramping model

A more sophisticated approach is presented in this paragraph. The thruster model is not perfectly fitting reality as the continuity of the fuel rate derivative is not assured. Despite that, a fist order approximation of the ramping up and down of the fuel rate can be evaluated without entering into details of a complex modeling. The thruster has a time interval $\Delta\, t_{\text{resp}}$ where the its valve cannot provide the needed amount of fuel and, as a consequence, a straight line transient connects the zero state to the steady one. The mathematical expression of this model is:

$$\boldsymbol{F}(t) = \begin{cases} I_{\text{sp}}\, g_0\, \dot{m}_{\text{fuel}}\, \frac{\boldsymbol{v}_{\text{exh}}}{v_{\text{exh}}}\, (t - t_{\text{in}\,\text{fir}}) & \text{if} \quad t_{\text{in}\,\text{fir}} \leq t \leq t_{\text{in}\,\text{fir}} + \Delta\, t_{\text{resp}} \\ I_{\text{sp}}\, g_0\, \dot{m}_{\text{fuel}}\, \frac{\boldsymbol{v}_{\text{exh}}}{v_{\text{exh}}} & \text{if} \quad t_{\text{in}\,\text{fir}} + \Delta\, t_{\text{resp}} < t \leq t_{\text{fin}\,\text{fir}} \\ I_{\text{sp}}\, g_0\, \dot{m}_{\text{fuel}}\, \frac{\boldsymbol{v}_{\text{exh}}}{v_{\text{exh}}}\, (t_{\text{fin}_{\text{fir}}} + \Delta\, t_{\text{resp}} - t) & \text{if} \quad t_{\text{fin}\,\text{fir}} < t \leq t_{\text{fin}\,\text{fir}} + \Delta\, t_{\text{resp}} \\ 0 & \text{otherwise} \end{cases} \tag{114}$$

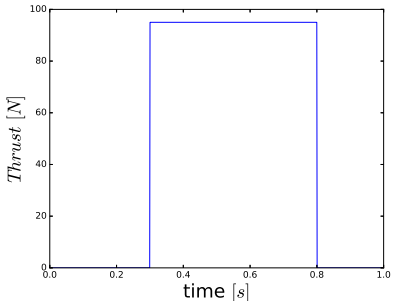

(a) Thrust

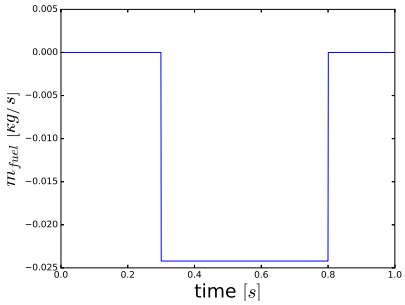

(b) $\dot{m}_{\text{fuel}}$

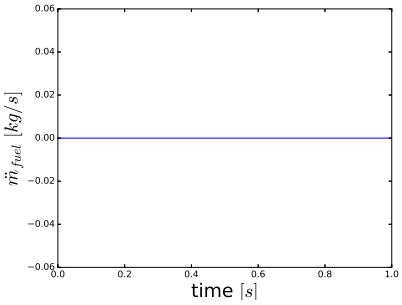

(c) $\ddot{m}_{\text{fuel}}$

Figure 10: Characteristics of the impulsive thruster firing from $t = 0.3\ s$ until $t = 0.8\ s$. In the shown simulation: $I_{\text{sp}} = 400\ s$ and $g_0 = 9.81\ \frac{m}{s^2}$.

where $\Delta\, t_{\text{resp}}$ has been previously defined. In Figures 11, the main properties of the thruster are presented for a $0.5\, s$ firing interval.

9 Numerical Implementation

The numerical resolution of the highly coupled system of equations 29 and 55 has been performed by a 4^{th} Runge-Kutta fixed step method.
During all propagation, the control to be applied to the spacecraft has not been updated each time step but it has been modified once the time was a multiple of the control update period T_{contr}, i.e. $t = n\, T_{\text{contr}}$ where $n \in \mathbb{N}^+$. This has been done in order to create a more reality-based simulation and to evaluate the importance of delays and discretization of the control law. The pseudo-code of this part of the program can be found in algorithm 1.

It must be underlined, on the one hand, that the asymptotic stability proof introduced in the previous paragraph is valid only in the continuous case. On the other, if the control update period T_{contr} is as fast as the internal dynamics of the

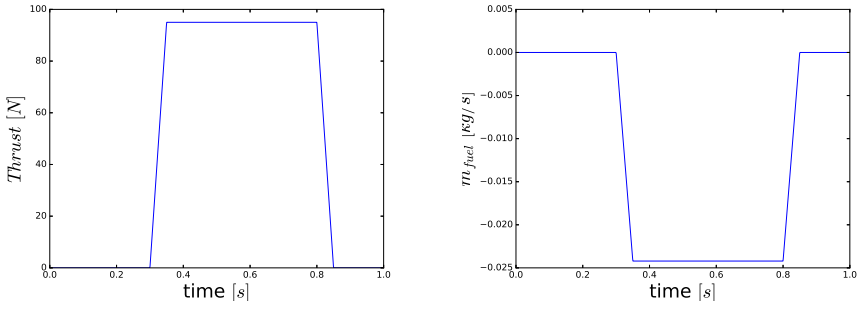

(a) Thrust

(b) $\dot{m}_{\text{fuel}}$

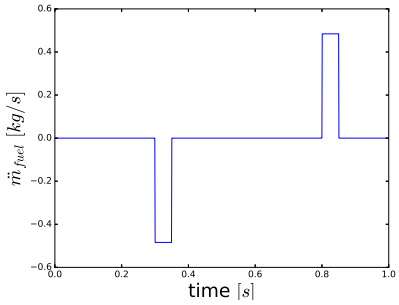

(c) $\ddot{m}_{\text{fuel}}$

Figure 11: Characteristics of the ramping thruster firing from $t = 0.3\ s$ until $t = 0.8\ s$. In the shown simulation: $I_{\text{sp}} = 400\ s$, $g_0 = 9.81\ \frac{m}{s^2}$ and $\Delta\, t_{\text{resp}} = 50\ ms$.

Data: X_0, t_0, t_{fin}, dt
Result: t, X
while $t < t_{fin}$ **do**
  if $t = n\, T_{contr}$ **then**
    $\boldsymbol{u} = -K\, \boldsymbol{\sigma}_{\mathcal{B}/\mathcal{R}} - P\, \boldsymbol{\omega}_{\mathcal{B}/\mathcal{R}}$;
    Compute forces according to the given trusters' configuration;
  end
  Integration of the EOMs;
  $t = t + dt$
end

Algorithm 1: Control update function

system and the state does not evolve rapidly when the control is kept constant , the system can be commanded by the control strategy exposed before. Moreover, in a real orbiting spacecraft the angular velocity of the satellite will never surpass

few degrees per second during its operation life and, as a consequence, the previous hypothesis is well verified and justified.
The function to be integrated is summarized with a pseudo-code in the algorithm 2 where the state variable derivatives are computed according with the given variables.

Data: m_{hub}, $[I]_{\text{hub},\,Bc}$, $\boldsymbol{r}_{Bc/B}$, $\boldsymbol{r}_{Fc_i/B}$, Tanks' Geometry, g_0, I_{sp_j}, $\boldsymbol{r}_{N_j/B}$, A_{noz_j}, $[BM]_j$, $[A]$, Thrusters' forces and firing times, $\boldsymbol{L}_{\text{ext},\,B}$, $\boldsymbol{F}_{\text{ext}}$
Result: $\dot{\boldsymbol{\omega}}_{\mathcal{B}/\mathcal{N}}$, $\dot{\boldsymbol{\sigma}}_{\mathcal{B}/\mathcal{N}}$, $\ddot{\boldsymbol{r}}_{B/N}$, $\dot{\boldsymbol{r}}_{B/N}$
Control the coherence of the given variable;
foreach *Thruster j* **do**
  Compute provided force j;
  Compute $\dot{m}_{\text{noz}_j}$ and $\ddot{m}_{\text{noz}_j}$;
end
Compute total thrust and trust's torque;
Compute $\dot{m}_{\text{fuel}_j}$ and $\ddot{m}_{\text{fuel}_j}$;
foreach *Tanks i* **do**
  Compute $\Delta\,\boldsymbol{r}_{Fc_i/B}$, $\boldsymbol{r}'_{Fc_i/B}$, $\boldsymbol{r}''_{Fc_i/B}$, $[I]_{\text{fuel},\,Fc_i}$ and $[I]'_{\text{fuel},\,Fc_i}$;
end
Compute $\boldsymbol{c}$, $\boldsymbol{c}'$ and $\boldsymbol{c}''$;
Compute $[I]_{\text{sc},\,B}$ and $[K]$;
Solve numerically the EOMs;

Algorithm 2: EOMs integrable function

Finally, this function is called each time step in the propagator to evaluate the state variables, i.e. rotational and translational states.

10 Results

In the present section the results obtained by the developed method, implemented in a Python environment, in different cases.
Firstly simulations will be shown to provide a way to validate the present model, where neither the angular momentum nor the energy are constant, and successively a series of fuel demanding maneuvers will be exposed in order to underline the importance to take into account the mass depletion for high-accuracy pointing, simulation and control law design.

10.1 Axial-symmetric rocket

The following simulations have been performed to reproduce the results outlined in [7] and validate the model.
The spacecraft under study is an axial-symmetric rocket represented in figure 12 where the geometrical feature of the launcher are shown.

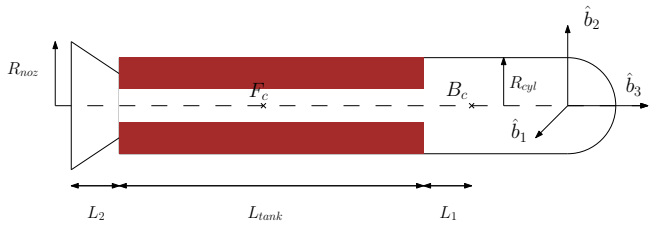

Figure 12: Geometrical properties of the axial-symmetrical rocket

The numerical values used in the simulations have been chosen accordingly with the NASA publication [7]. In the paper dimensionless variables are used and their primitive definitions can be found in the following formulas.

$$\beta = \frac{R_{\text{noz}}}{R_{\text{cyl}}} \qquad \delta_1 = \frac{L_1}{R_{\text{cyl}}} \qquad \delta_2 = \frac{L_2}{R_{\text{cyl}}} \qquad \delta = \frac{L}{R_{\text{cyl}}} \tag{115}$$

$$\psi = \frac{m_{\text{hub}}}{m_{\text{fuel}_0}} \qquad \gamma_1 = \frac{k_{\text{hub}_{12}}}{R_{\text{cyl}}} \qquad \gamma_2 = \frac{k_{\text{hub}_3}}{R_{\text{cyl}}} \qquad \alpha = \frac{\dot{m}_{\text{fuel}}}{m_{\text{fuel}_0}}$$

where $k_{\text{hub}_{12}}$ is the hub's gyration radius of the $\hat{\boldsymbol{b}}_1$ or the $\hat{\boldsymbol{b}}_2$ about the Bc point and k_{hub_3} is the hub's gyration radius of the $\hat{\boldsymbol{b}}_3$ about the same point. The numerical dimensionless coefficients' values are reported in table 1.

δ_1	δ_2	γ_1	γ_2	α
2	3	1.2	1	0.01

Table 1: Dimensionless parameters for the axial-symmetrical rocket simulation

The value of the not given constants will be presented section per section as they change from simulation to simulation.

10.1.1 Centrifugal burn

In this section a centrifugal burn simulation is presented both for the spinning rate $\boldsymbol{\omega}_{\mathcal{B}/\mathcal{N}_z}$ and for the traversal angular velocity $\boldsymbol{\omega}_{\mathcal{B}/\mathcal{N}_{x\,y}}$. These two quantities can be defined as follows:

$$\boldsymbol{\omega}_{\mathcal{B}/\mathcal{N}_z} = \boldsymbol{\omega}_{\mathcal{B}/\mathcal{N}} \cdot \hat{\boldsymbol{b}}_3 \qquad \boldsymbol{\omega}_{\mathcal{B}/\mathcal{N}_{x\,y}} = \sqrt{\left(\boldsymbol{\omega}_{\mathcal{B}/\mathcal{N}} \cdot \hat{\boldsymbol{b}}_1\right)^2 + \left(\boldsymbol{\omega}_{\mathcal{B}/\mathcal{N}} \cdot \hat{\boldsymbol{b}}_2\right)^2} \tag{116}$$

It can be seen in figures 13 the behavior of the angular velocity all along the simulation.
On the one hand, the β parameter, i.e. the ratio between the nozzle's radius and the tank's one, has been changed to show the possibility of diverging solutions in the case of the spin rate. In fact, in those cases the quantity of angular momentum transported from the particles is fewer than the tank's variation of

the latter and, as a consequence, the spin rate increases.
On the other, the δ parameter, i.e the ration between the rocket radius and the tank's length, has been changed and, as shown in figure 13(b), the solution is always converging to a stable null state.

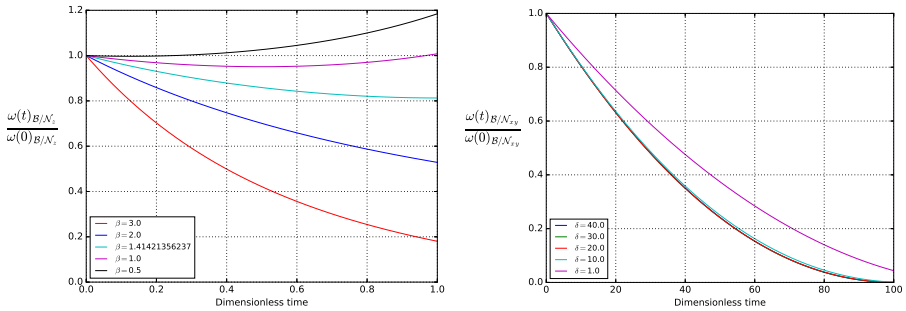

(a) Spin rate evolution in time

(b) Traversal rate evolution in time

Figure 13: Angular velocity $\boldsymbol{\omega}_{\mathcal{B}/\mathcal{N}}$ in the centrifugal burning cylinder simulation.

Moreover, $\delta = 10$ and $\psi = 2$ in the on-axis simulation and $\beta = 1$ and $\psi = 10$ in the out-of-axis one.

10.1.2 Uniform burn

In this section the uniform burning cylinder simulation are presented in figures 14.
It can be underlined that the solution in less steep and convex as the radius of the fuel inside the tank does not change all along the simulation. In particular, no spin rate variation is evidenced if $\beta = 1$ as the tank's radius is equal to the nozzle's one and, consequently, the amount of angular transported and his variation inside the tank are exactly the same.
On the contrary, the transversal angular velocity converges more rapidly as the fuel mass distribution is not affecting the convergence of the out-of-axis velocity.
Finally, $\delta = 10$ and $\psi = 2$ in the on-axis simulation and $\beta = 1$ and $\psi = 15$ in the out-of-axis one.

10.2 On-orbit spacecraft simulations

As this research has been developed to fulfill the necessity of high-accuracy simulations in spacecraft dynamics, the following simulations take into account the gravity field experienced around the Earth. A simple two-body-problem gravity field has been considered and implemented in the code and no gravity torque perturbation has been included in order to underline the effect due to mass variation and to simplify the presented scenarios.
Moreover, the coherence of the simulated maneuvers has been checked by the

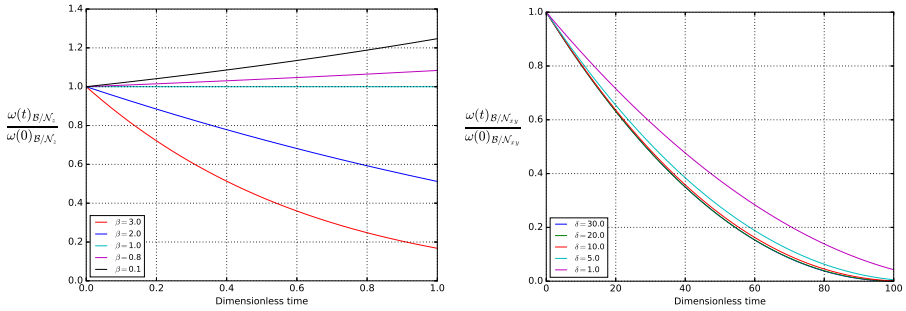

(a) Spin rate evolution in time (b) Traversal rate evolution in time

Figure 14: Angular velocity $\boldsymbol{\omega}_{\mathcal{B}/\mathcal{N}}$in the centrifugal burning cylinder simulation.

analysis of the constancy of orbital elements $[a,\, e,\, i,\, \omega,\, \Omega,\, \nu]$ whose numerical computation has been widely exposed in [10].

10.2.1 De-tumbling maneuver

In this scenario a tumbling at high angular velocity satellite is stabilized throughout the control strategy exposed before. The satellite has a 12-ADC nozzle cluster disposed in a symmetric configuration to in order to obtain a pure torque and the spacecraft is orbiting around the Earth at low altitude in a circular orbit. The orbital parameters of the chosen orbit are shown in table 2.

$a\ [km]$	$e\ [\,]$	$i\ [^\circ]$	$\omega\ [^\circ]$	$\Omega\ [^\circ]$
6578.0	0.0	0.0	0.0	0.0

Table 2: Initial orbital element for the de-tumbling maneuver

$m_{\text{hub}}\ [kg]$	$I_{\text{hub},\, Bc_1\,1}\ \left[kg\,m^2\right]$	$I_{\text{hub},\, Bc_2\,2}\ \left[kg\,m^2\right]$	$I_{\text{hub},\, Bc_3\,3}\ \left[kg\,m^2\right]$
750.0	900.0	800.0	600.0
$I_{\text{sp}_j}\ [s]$ $\forall j \in [1,\, 12]$	$m_{\text{tank}_i}\ [kg]$ $\forall i \in [1,\, 2]$	$A_{\text{noz}_j}\ \left[m^2\right]$ $\forall j \in [1,\, 12]$	$R_{\text{tank}_i}\ [m]$ $\forall i \in [1,\, 2]$
300.0	100.0	0.07	0.5

Table 3: Geometrical characteristics of the satellite for the de-tumbling maneuver

The simulation characteristics and the geometrical features are shown in tables 2 and 4 respectively. The values in table 4 have been chosen according to

$t_{\text{in}}\,[s]$	$t_{\text{fin}}\,[s]$	$\Delta\,t\,[s]$	$T_{\text{contr}}\,[s]$
0.0	200.0	0.01	1.0

$\boldsymbol{r}_{B/N_0}\,[m]$	$\dot{\boldsymbol{r}}_{B/N_0}\,[m\,s^{-1}]$	$\boldsymbol{\sigma}_{\mathcal{B}/\mathcal{N}_0}\,[\,]$	$\boldsymbol{\omega}_{\mathcal{B}/\mathcal{N}_0}\,[rad\,s^{-1}]$
$[a,\,0,\,0\,]^T$	$\left[0,\,\sqrt{\frac{\mu}{a}},\,0\,\right]^T$	$[0,\,0,\,0\,]^T$	$[-1,\,1,\,1\,]^T$

$\mu\,[km^3\,s^{-3}]$	$\boldsymbol{\sigma}_{\mathcal{R}/\mathcal{N}}\,[\,]$	$\boldsymbol{\omega}_{\mathcal{R}/\mathcal{N}}\,[rad\,s^{-1}]$
398600.0	$[0,\,0,\,0\,]^T$	$[0.002,\,0,\,0\,]^T$

Table 4: De-tumbling simulation parameters

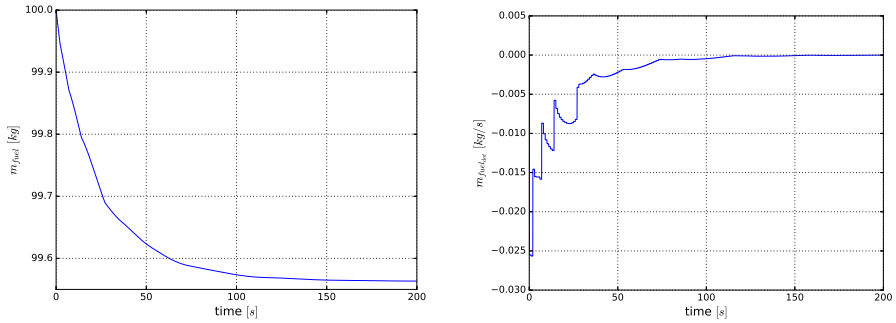

(a) m_{fuel} (b) $\dot{m}_{\text{fuel}}$

Figure 15: Mass variation during the de-tumbling simulation.

real industrial designs and realistic configurations of low orbit satellite.
As far as the control concerns, the feedback law gains have been fixed to achieve a stable system without let the mass flow rates to be too high and unrealistic thanks to the approach developed in [8] that is based on the study of the linearized dynamic. In this simulation $K = 20$ and $P = 50$.
The numerical results are shown in figures 16 where the modulus of the computed angular velocity and the projection on each $\mathcal{B}-$frame axis can be analyzed. On the one hand, it must be underlined that the solution achieves the right angular velocity $\boldsymbol{\omega}_{\mathcal{B}/\mathcal{N}}$ in less than $100\,s$. Moreover, despite no proof on asymptotic stability in case of a MRP feedback law, the system can be achieve the desired steady state as the system dynamics, i.e. the angular velocity, is not excessively rapid if compared to the control period T_{contr}. In fact, under the previously explained condition the state at $t = k\,T_{\text{contr}}$ is almost unchanged before the control is updated.
On the other, the path followed by the angular velocity in figure 16(a) is not the optimal time trajectory as the solution starts hovering around.
In figures 15 the mass flow rate and the mass variation during the de-tumbling

maneuver can be seen. The mass needed to de-tumble the satellite in case of a high angular velocity is less than $0.5\,kg$ per tank and the mass flow rate has its maximal value around $25\,g\,s^{-1}$. The nozzle mass rate is comparable with industrial designs and the maximal thrust provided by each nozzle is $T_{max} \simeq I_{\text{sp}}\, g_0\, \dot{m}_{\text{fuel}} = 73.5\,N$, tantamount to the forces provided by on-the-shelf component from an average size spacecraft.

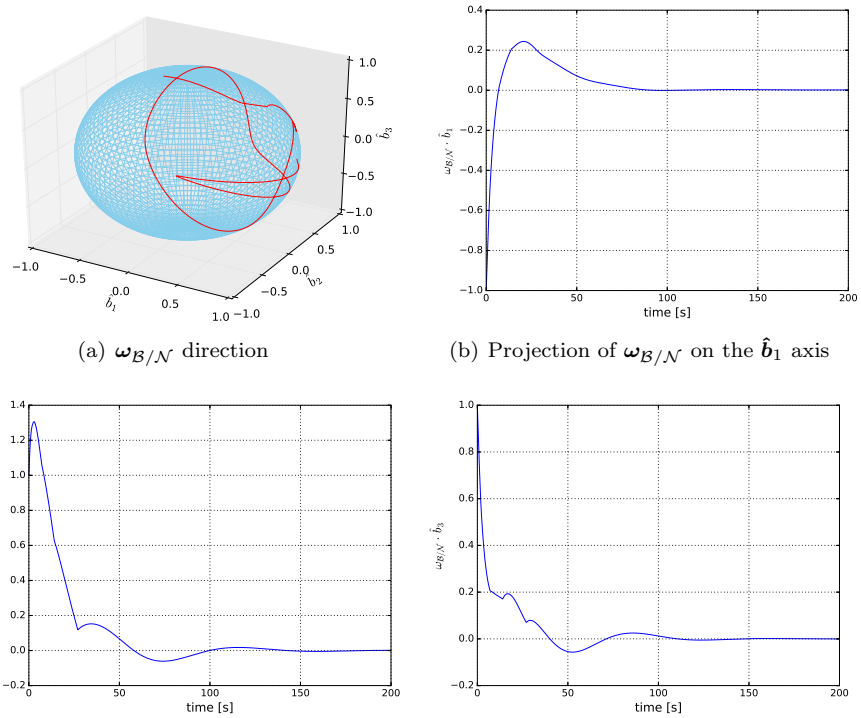

(a) $\boldsymbol{\omega}_{\mathcal{B}/\mathcal{N}}$ direction

(b) Projection of $\boldsymbol{\omega}_{\mathcal{B}/\mathcal{N}}$ on the $\hat{\boldsymbol{b}}_1$ axis

(c) Projection of $\boldsymbol{\omega}_{\mathcal{B}/\mathcal{N}}$ on the $\hat{\boldsymbol{b}}_2$ axis

(d) Projection of $\boldsymbol{\omega}_{\mathcal{B}/\mathcal{N}}$ on the $\hat{\boldsymbol{b}}_3$ axis

Figure 16: Angular velocity $\boldsymbol{\omega}_{\mathcal{B}/\mathcal{N}}$ in the de-tumbling case.

10.2.2 LEO-to-GEO maneuver

In this section a geostationary transfer maneuver from a LEO (Low Earth Orbit) and a GEO (Geostationary Earth Orbit) passing through an elliptic orbit, i.e. a Hohmann maneuver has been implemented. The orbital element of the three exposed orbits can be consulted in table 5.

By solving the dynamic equations, satellite's position and velocity have been simulated in order to compute the orbit elements and to control if the final orbit is the desired one. As equations of motion have been propagated each time step, a finite thrust approach must be implemented. Thanks to equation 111, the force to be applied must be computed knowing both the required $\Delta\, v$ and the length

	a $[km]$	e []	i [°]	ω [°]	Ω [°]
Low Earth Orbit	6578.0	0.0	0.0	0.0	0.0
Hohmann Transfer Orbit	24478.0	0.73126	0.0	90.0	0.0
Geostationary Earth Orbit	42378.0	0.0	0.0	0.0	0.0

Table 5: Orbital element for the Hohmann maneuver.

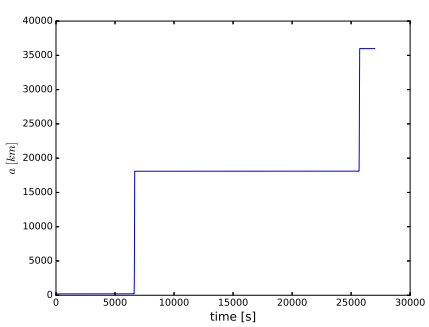

(a) Projection of $\boldsymbol{\omega}_{\mathcal{B}/\mathcal{N}}$ on the $\hat{\boldsymbol{b}}_1$ axis

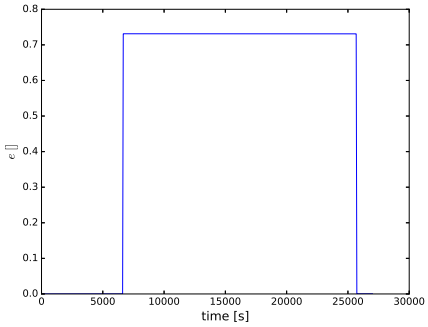

(b) Projection of $\boldsymbol{\omega}_{\mathcal{B}/\mathcal{N}}$ on the $\hat{\boldsymbol{b}}_2$ axis

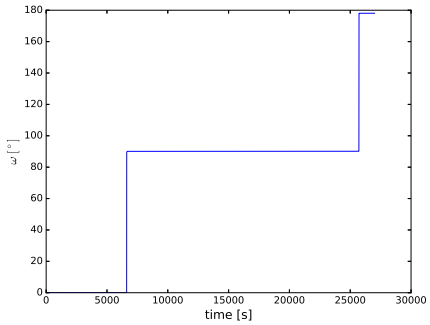

(c) Projection of $\boldsymbol{\omega}_{\mathcal{B}/\mathcal{N}}$ on the $\hat{\boldsymbol{b}}_3$ axis

Figure 17: Angular velocity $\boldsymbol{\omega}_{\mathcal{B}/\mathcal{N}}$ in the de-tumbling case.

of the time interval $\Delta\, t_{\text{man}}$ in which the thrusters are firing. Then, the thrusters switch on $\frac{\Delta\, t_{\text{man}}}{2}$ before the impulsive maneuver time and turn off $\frac{\Delta\, t_{\text{man}}}{2}$ after to maintain a symmetric maneuver enough close to the impulsive one. The simulated planar orbit elements are shown in figures 17.

In this scenario, the satellite has the same ADC-thrusters' cluster configuration and it is equipped with two bigger nozzle to perform the firing at the apogee and at the perigee of the elliptic orbit. The geometrical feature are presented in table 6.
Furthermore the initial conditions for the dynamic variables and the chosen simulation parameters are listed in table 7.

$m_{\text{hub}}\ [kg]$	$I_{\text{hub},\ Bc_{1\,1}}\ [kg\,m^2]$	$I_{\text{hub},\ Bc_{2\,2}}\ [kg\,m^2]$	$I_{\text{hub},\ Bc_{3\,3}}\ [kg\,m^2]$
750.0	900.0	800.0	600.0

$I_{\text{sp}_j}\ [s]$ $\forall j \in [1,\ 14]$	$m_{\text{tank}_i}\ [kg]$ $\forall i \in [1,\ 2]$	$A_{\text{noz}_j}\ [m^2]$ $\forall j \in [3,\ 14]$	$A_{\text{noz}_j}\ [m^2]$ $\forall j \in [1,\ 1]$	$R_{\text{tank}_i}\ [m]$ $\forall i \in [1,\ 2]$
300.0	700.0	0.07	0.2	0.5

Table 6: Geometrical characteristics of the satellite for the Hohmann transfer.

$t_{\text{in}}\ [s]$	$t_{\text{fin}}\ [s]$	$\Delta t\ [s]$	$T_{\text{contr}}\ [s]$
0.0	27000.0	0.01	1.0

$\boldsymbol{r}_{B/N_0}\ [m]$	$\dot{\boldsymbol{r}}_{B/N_0}\ [m\,s^{-1}]$	$\boldsymbol{\sigma}_{\mathcal{B}/\mathcal{N}_0}\ [\,]$	$\boldsymbol{\omega}_{\mathcal{B}/\mathcal{N}_0}\ [rad\,s^{-1}]$
$[a,\ 0,\ 0\,]^T$	$\left[0,\ \sqrt{\frac{\mu}{a}},\ 0\right]^T$	$[0,\ 0,\ 0\,]^T$	$[0.002,\ 0,\ 0\,]^T$

$\mu\ [km^3\,s^{-3}]$	$\boldsymbol{\sigma}_{\mathcal{R}/\mathcal{N}}\ [\,]$	$\boldsymbol{\omega}_{\mathcal{R}/\mathcal{N}}\ [rad\,s^{-1}]$
398600.0	$[0,\ 0,\ 0\,]^T$	$[0.002,\ 0,\ 0\,]^T$

Table 7: Hohmann transfer simulation parameters

The numerical results of the simulation are presented in figures 18 and 19. Three scenarios are analyzed and simulated:

- The Update-Only simulation is the easiest one that does not consider the influence of mass depletion on the system except for the instantaneous position of the center of mass, the instantaneous mass and the instantaneous inertia. No dynamic effects are taken into account and the only influence the mass variation has on the system is to update the parameters every time step.
- The No-Control simulation considers the equations inferred in the previous sections but does not take into account considering the effect of the control law on the system. This simulation is useful to compare the developed model with the Update-Only one.
- The Active-Control simulation propagates the complete system of equation considering the previously exposed active control.

In the two figures 18(a) and 18(b) the projection of the $\boldsymbol{\omega}_{\mathcal{B}/\mathcal{N}}$ is shown. In the first one, the complete $27000\,s$ simulation is presented to compare the previously listed simulations. By comparing the Update-Only model with the No-Control one, it can be easily seen a difference in the angular velocity of the system caused by the dynamical effects introduced by the mass depletion. The

fact that the angular variation is negative and its magnitude are due to the thrusters' cluster configuration, both in term of position and geometry, and the tanks' location and dimension as equation 53 shows. Obviously changing one of the two features will lead to a different solution in terms of amplitude and sign. In this particular case, the error introduced by mass depletion is about 4 %. In the second figure, a zoom of the first maneuver is introduced to let the reader to have an idea about overshoots and oscillation of the system with the chosen control gains ($K = 20$ and $P = 50$).
Finally, the other projections of the $\boldsymbol{\omega}_{\mathcal{B}/\mathcal{N}}$ vector will not be analyzed as the symmetric configuration, both in terms of thrusters and in terms of mass, does not create any type of torque on the system and they remain null all along the simulation.

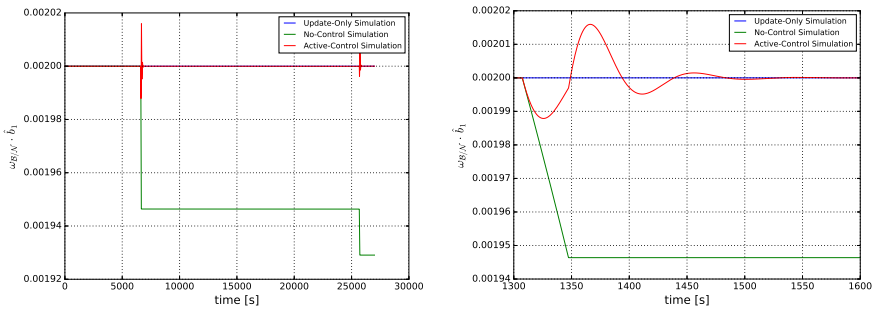

(a) General behavior for the coplete simuation.

(b) Details for the first firing period.

Figure 18: Projection of $\boldsymbol{\omega}_{\mathcal{B}/\mathcal{N}}$ on the $\hat{\boldsymbol{b}}_3$ axis.

Moreover, in figures 19(a) and 19(a) the mass variation of the system is shown.

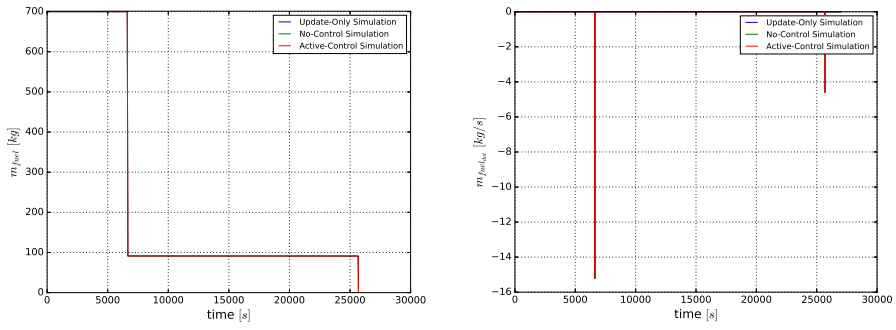

(a) m_{fuel}

(b) $\dot{m}_{\text{fuel}}$

Figure 19: Mass variation during the Hohmann maneuver simulation.

11 Conclusions

In this report a review of the previous works on mass variable system has been firstly presented specifying the needed hypothesis where necessary. Moreover, a novel and compact form of the EOMs has been introduced in the case of a realistic multi-tank and multi-thruster configuration that provides rapid and efficient formulation to perform simulations.
On the one hand, some limiting hypothesis have been introduced that does not allow the EOMs to consider the effect of whirling motions or fuel distribution system. On the other, the chosen formulation underlines the main effects caused by the mass depletion and the modular approach provides an easy way to introduce other causes of the barycenter displacements, such as panels' deployment or flexible structures, without loss of generality.
Secondly, some example of tanks and thrusters have been inferred to underline the modularity of the model and his capability to simulate complex behaviors, as the emptying tank model, once the user needs.
Finally, the importance of considering such effects has been proven by comparing a solution where the dynamic parameters are just updated each time step and the complex model simulation. This has led to an error of the 4 % on the spacecraft angular velocity with the chosen geometrical feature. This model error could lead to shorter time life and hastened de-saturation maneuver or cause inaccurate pointing and unpredicted errors in orientation and position.
Future works could consider the influence of whirling motion using a simple formulation or introduction of reaction wheels to simulate complex de-saturation maneuvers.

References

[1] R. W. Fox, A. T. McDonald, and P. J. Pritchard, *Introduction to fluid mechanics*, Vol. 7. John Wiley & Sons New York, 1985.

[2] F. White, *Fluid Mechanics*. McGraw-Hill series in mechanical engineering, McGraw Hill, 2011.

[3] B. Munson, A. Rothmayer, and T. Okiishi, *Fundamentals of Fluid Mechanics, 7th Edition*. John Wiley & Sons, Incorporated, 2012.

[4] J. F. Thorpe, "On the momentum theorem for a continuous system of variable mass," *Am. J. Phys*, Vol. 30, 1962, pp. 637–640.

[5] M. B. Quadrelli, J. Cameron, B. Balaram, M. Baranwal, and A. Bruno, "Modeling and Simulation of Flight Dynamics of Variable Mass Systems," 2014.

[6] M. I. Marmureanu and I. Fuiorea, "Attitude Dynamics of a Spinning Rocket with Internal Fluid Whirling Motion," *INCAS Bulletin*, Vol. 6, No. 2, 2014, p. 75.

[7] F. O. Eke, "Dynamics of variable mass systems," 1998.

[8] H. Schaub and J. L. Junkins, *Analytical Mechanics of Space Systems*. Reston, VA: AIAA Education Series, 3rd ed., 2014, 10.2514/4.102400.

[9] C. Bruccoleri and D. Mortari, "MRAD: Modified rodrigues vector Attitude determination," *The Journal of the Astronautical Sciences*, Vol. 54, No. 3-4, 2006, pp. 383–390.

[10] D. A. Vallado, *Fundamentals of astrodynamics and applications*, Vol. 12. Springer Science & Business Media, 2001.